Comparing high-latitude thermospheric winds from FPI and CHAMP accelerometer measurements

Anasuya Aruliah[1,] Matthias Förster[2,3], Rosie Hood[1], Ian McWhirter[1], Eelco Doornbos[~~4~~3,~~5~~4]

[1]Atmospheric Physics Laboratory, University College London, Gower Street, London, WC1E 6BT, UK
[2]Helmholtz-Zentrum Potsdam, GFZ German Research Centre for Geosciences, Telegrafenberg, 14473 Potsdam, Germany
[3]Max Planck Institute for Solar System Research (MPS), Justus-von-Liebig-Weg 3, 37077 Göttingen, Germany
[~~4~~3]Old affiliation: Faculty of Aerospace Engineering, Delft University of Technology (TU Delft), Kluyverweg 1, 2629 HS Delft, The Netherlands
[~~5~~4]Current affiliation: Royal Netherlands Meteorological Institute (KNMI), Utrechtseweg 297, 3731 GA De Bilt, The Netherlands

Correspondence to: Anasuya Aruliah (a.aruliah@ucl.ac.uk), ~~and~~ Matthias Förster (mfo@gfz-potsdam.de) and Eelco Doornbos (eelco.doornbos@knmi.nl)

Abstract. It is generally assumed that horizontal wind velocities are independent of height above the F_1-region (> 300 km) due to the large molecular viscosity of the upper thermosphere. This assumption is used to compare two completely different methods of thermospheric neutral wind observation, using two distinct locations in the high-latitude Northern Hemisphere. The measurements are from ground-based Fabry-Perot Interferometers (FPI), and from in-situ accelerometer measurements onboard the CHAMP satellite, which was in a near polar orbit. The UCL KEOPS FPI is located in the vicinity of the auroral oval at the ESRANGE site near Kiruna, Sweden (67.8°N, 20.4°E). The UCL Longyearbyen FPI is a polar cap site, located at the Kjell Henriksen Observatory on Svalbard (78.1°N, 16.0°E). The comparison is done in a statistical sense, comparing a longer time series obtained during nighttime hours in the winter months (~~November to January~~DOY 300-65); with overflights of the CHAMP satellite between 2001 and 2007 over the observational sites, within ±2° latitude (±~~220~~ 230 km horizontal range). The FPI is assumed to measure the line-of-sight winds at ~240 km height, i.e. the peak emission height of the atomic oxygen 630.0 nm emission. The cross-track winds are derived from state-of-the-art precision accelerometer measurements at altitudes between ~450 km (in 2001) to ~~~330~~ 350 km (in 2007); i.e. 100-200 km above the FPI wind observations. We show that CHAMP winds at high latitudes are ~~systematically~~ typically 1.5-2 times larger than FPI winds. In addition to testing the consistency of the different measurement approaches, the study aims to clarify the effects of viscosity on the height dependence of thermospheric winds.

1 Introduction

Global circulation models (GCM) of the upper atmosphere (80-600 km altitude) appear in two forms: climatologies based on empirical measurements, and theoretical models that calculate ~~the~~ atmospheric conditions using the principles of physics and chemistry. These models are important for space weather studies

Style Definition: Normal: Justified, Line spacing: 1.5 lines

Formatted: English (United Kingdom)

Formatted: Plain Text, Adjust space between Latin and Asian text, Adjust space between Asian text and numbers

Formatted: Font: (Default) Times New Roman, 10 pt, Not Bold, Font color: Auto

Formatted: Adjust space between Latin and Asian text, Adjust space between Asian text and numbers and are also applied in understanding and predicting drag on low-altitude satellites, space debris, and the study of re-entry of near Earth objects. The theoretical and empirical models rely on observations from ground-based instruments around the world and global observations by satellites to provide constraints and boundary conditions. In particular, models must account for energy from sources external to the upper atmosphere (i.e., direct solar radiation, particle precipitation and heat flow from above; radiative, conductive and convective heating from below; the magnetospheric electrodynamic driver at high-latitudes), which is divided between acceleration of the gas and heating. The empirical evidence for the energy budget ~~is~~ can be provided by observations of winds and temperatures.

The use of accelerometers on satellites to measure thermospheric winds had previously been reported quite rarely (Marcos and Forbes, 1985; Forbes et al., 1993). Over the last few years CHAMP and GOCE winds have been reported (e.g. Förster et al., 2008; Doornbos et al., 2010). The advantage of this technique consists in the fairly direct in-situ measurement, with relatively high spatial (temporal) resolution, of the cross-track wind component along the orbital track with only a limited number of special assumptions for the data interpretation. Adding more satellites (e.g., GRACE and GRACE-FO), should allow better full wind vector reconstructions in terms of statistical averages (Förster et al., 2008; Förster et al., 2017) as well as parameterized statistical studies of the upper thermosphere dynamics in the near future. As a result, it makes it imperative that the derived winds are correct because satellites provide global coverage of the upper atmosphere, unlike the small number of ground-based instruments currently in existence. The larger databases and global coverage of the satellites will particularly influence a semi-empirical model such as the Horizontal Wind Model (Drob et al., 2015), which is commonly used as a climatology of winds to provide initial boundary conditions and validation for physics-based global circulation models (GCMs).

In this paper we show that upper thermospheric winds measured by the CHAMP satellites are ~~systematically~~ typically 1.5 to 2 times larger than those measured by ground-based Fabry-Perot Interferometers (FPIs) at an auroral site and ~~p~~polar cap site. It is imperative to know whether this discrepancy is real (i.e. there is a variation of speed with ~~r~~respect to height), or whether we have uncovered a problem of the absolute scaling of wind measurements by comparing FPIs with CHAMP. With incorrect scaling, there arises a problem of distortion of energy budget ~~c~~calculations of the upper atmosphere~~ as demonstrated below~~. A precise estimation of energy supply to the system is hindered essentially, because the partitioning of kinetic and thermal energy channels becomes obscured. The acceleration of the neutral air in 3-D space with respect to the active driver of the plasma motion is important to estimate, for instance, the Joule heating rate as one of the most important thermal energy inputs. This has a knock-on effect on the calculation of the absolute density of the gas, which is an important parameter used in, for example, satellite orbit calculations.

~~Consider a very simple simplified argument where the added energy per unit volume is δE, and the wind measured by the satellite and FPI are U_{sat}, and U_{FPI}, respectively. The energy is redistributed between a change in kinetic energy and heating of the atmosphere. If the gas has density ρ, and is accelerated from being initially stationary to speed U, then the energy redistribution is given by Eq. (1)~~

Formatted: Adjust space between Latin and Asian text, Adjust space between Asian text and numbers
Formatted: Font: (Default) Times New Roman
Formatted: Font: (Default) Times New Roman
Formatted: Font: (Default) Times New Roman
Formatted: Font: (Default) Times New Roman
Formatted: Font: (Default) Times New Roman
Formatted: Font: (Default) Times New Roman
Formatted: Font: (Default) Times New Roman
Formatted: Font: (Default) Times New Roman
Formatted: Font: (Default) Times New Roman
Formatted: Font: (Default) Times New Roman
Formatted: Font: (Default) Times New Roman

$$\delta E = \frac{1}{2}\rho U^2 + \rho C_p \delta T \qquad (1)$$

Let us assume that the satellite and FPI are measuring the same volume of gas, but are not absolutely calibrated. Let δT_{sat} and δT_{FPI} be the change in temperature due to heating as measured by the satellite and FPI, respectively. Thus the change in energy is given by Eq. (2), assuming a mean density $\bar{\rho}$ ρ during this process.

$$\delta E = \frac{1}{2}\bar{\rho} U_{sat}^2 + \bar{\rho} C_p \delta T_{sat} = \frac{1}{2}\bar{\rho} U_{FPI}^2 + \bar{\rho} C_p \delta T_{FPI} \qquad (2)$$

Consider if the measurements from the satellite and FPI are such that $U_{sat} = 2U_{FPI}$, i.e. either the satellite or the FPI (or both) are wrongly calibrated, then substituting for U_{sat} in Eq. (2), and rearranging both equations, leads to Eq. (3).

$$4\delta T_{FPI} - \delta T_{sat} = \frac{3\delta E}{\rho C_p} \qquad (3)$$

Thus Eq. (3) demonstrates that for positive δE (i.e. heating), the inferred satellite temperatures are appear to be larger than the FPI temperatures (e.g. if $\delta E \approx 0$, then $\delta T_{sat} \approx 4\delta T_{FPI}$). In other words, by applying the satellite wind measurements, the implication isy that more energy is put into heating the gas, and less into accelerating the gas., Meanwhile applying the FPI wind measurements would indicate the reverse. This would result in a mismatch between modelled and observed temperature changes. The FPI can measure temperatures to test this, as will be done in a future study. The temperature discrepancy would also have a knock-on effect on the calculation of density ρ of the gas as determined by the satellites, or by ground-based FPIs, since $\delta p = nk_B\delta T$, where k_B is the Boltzmann constant and n is the number density of the gas particles. Note that this argument for a point localised measurement is oversimplified. The purpose is to highlight the repercussions of overestimating (or underestimating) the neutral wind on the division of energy between heating and acceleration of the neutral gas. The conservation of momentum, energy, and continuity must be satisfied, and oOwing to the high molecular viscosity and heat conductivity, the whole air column above the measurement location should be accelerated and heated.

Formatted: Font: (Default) Times New Roman, Not Bold

2 The CHAMP accelerometer data

The challenging mini-satellite payload (CHAMP) was managed by the GFZ German Research Centre for Geosciences of the Helmholtz Centre Potsdam. This mission was designed to perform detailed studies of the Earth's gravitational and magnetic field with unprecedented accuracies and space/time resolutions as well as GPS atmosphere and ionosphere profiling. The spacecraft was launched in July 2000 into a circular near-polar orbit with 87.3° inclination at an initial altitude of ~460 km (Reigber et al., 2002). Its orbital altitude gradually decayed to ~400 km in 2003 and ~330 km in 2008, and ended in September 2010.

One key scientific instrument onboard CHAMP was a triaxial accelerometer. It was located at the spacecraft's center of mass and effectively probed the in-situ air drag. Thermospheric mass density and cross-track neutral wind can be obtained from the drag acceleration observations. It is very difficult to determine the error estimate because it depends on several variables as discussed in Doornbos et al. (2010) and shown in Table 5 from Visser et al. (2019). This indicates that for force-derived winds, the largest sensitivity is to energy accommodation, which is of the order of several tens of ms^{-1}.

A first analysis of the high-latitude thermospheric wind circulation in dependence on the IMF orientation was performed by Förster et al. (2008) using the preliminary methodology of cross-track wind estimations from accelerometer data as described in Liu et al. (2006). Förster et al. (2011) then presented an overview of the average transpolar thermospheric circulation in terms of the vorticity. Here, they made use of the newly calibrated and re-analysed data set that resulted from an ESA study, initiated for the Swarm satellites mission launched in November 2013 (Helleputte et al., 2009). The CHAMP neutral wind data, based on the cross-track accelerometer measurements, are available via the data repository at the GFZ Potsdam (Förster and Doornbos, 2019).

Formatted: Normal, Don't adjust space between Latin and Asian text, Don't adjust space between Asian text and numbers

Formatted: Font: (Default) Times New Roman

As pointed out by Doornbos et al. (2010), the along-track wind is not resolvable because it induces a similar signal in the acceleration as the density variation. This wind component is ignored, or the value from an empirical wind model is used, because the along-track wind is a relatively small magnitude in comparison with the satellite speed of 7.6 km s^{-1}. The empirical wind model used is, for example, HWM90 (Hedin et al., 1991) or its latest edition HWM14, as published by Drob et al. (2015). In polar areas the along-track wind velocity can achieve up to 10% of the satellite speed. Consequently, the along-track mass density estimation can have an error of about 20% in the polar latitudes, because the acceleration is proportional to the wind velocity squared (e.g., Doornbos et al., 2010). But it is less easy to estimate the error in the cross-track wind in the polar region due to considerably smaller acceleration signals. There are also systematic contributions from other sources such as gas-surface interactions, surface properties, spacecraft shape, spacecraft attitude and radiation pressure accelerations, which make the satellite aerodynamic coefficients difficult to resolve (see Doornbos et al., 2010, and the error budget in Appendix A of that paper; Mehta et al., 2017 and March et al., 2018). The pre-processed data of the accelerometer were re-sampled to 10-sec averages for the further use in this study. Measurements of 10-sec cadence correspond to a spatial separation of 76 km or about 2/3° in latitude between the individual data points.

3 The Fabry-Perot Interferometer data

The advantage of using Fabry-Perot Interferometers is that they make direct measurements of thermospheric wind speeds using only a few instrumental or geophysical assumptions. They are also generally reliable instruments that can be left to run for months at a time. The FPIs operated by University College London are located at the Kiruna Esrange Optical Platform System (KEOPS) in northern Sweden; and on the island of

Svalbard at the Adventdalen Observatory (before November 2006), from which it was moved to the Kjell Henriksen Observatory (after November 2006). The geographic and geomagnetic coordinates of these two stations are given in Table 1 for Kiruna (KEOPS) and Table 2 for Longyearbyen (Svalbard). The Altitude-Adjusted Corrected Geomagnetic Coordinates (AACGM) are obtained from http://sdnet.thayer.dartmouth.edu/aacgm/aacgm_calc.php#AACGM (Shepherd, 2014). A date of 15 December 2002 was used, for an altitude of 240 km. Owing to the large field-of-view of the FPIs (see later) the locations of the volumes observed by the FPIs in the East and West look directions are also given, and the corresponding MLT.

Formatted: Font: Not Italic

Table 1

FPI Site	Geographic coordinates	AACGM geomagnetic coordinates for 15 Dec 2002 at 240 km altitude	AACGM magnetic local time (MLT) midnight in UT
Kiruna (KEOPS)	67.87°N, 21.03°E	65.08°N, 103.32°E	1.860 UT~~0 hrs~~
Kiruna (KEOPS) EAST	67.87°N, 26.6°E	64.8°N, 107.8°E	2.16 UT
Kiruna (KEOPS) WEST	67.87°N, 15.5°E	65.4°N, 98.9°E	1.57 UT

Formatted Table

Table 2

FPI Site	Geographic coordinates	AACGM geomagnetic coordinates for 15 Dec 2002 at 240 km altitude	AACGM magnetic local time (MLT) midnight in UT
Longyearbyen (KHO after 2006)	78.15°N, 16.04°E	75.38°N, 111.80°E	2.43 UT
Longyearbyen EAST (KHO after 2006)	78.15°N, 33.6°E	74.4°N, 123.6°E	3.21 UT
Longyearbyen WEST (KHO after 2006)	78.15°N, -1.5°E	76.8°N, 100.3°E	1.66 UT

Formatted Table

Formatted Table

Longyearbyen (Adventdalen before 2006)	78.19°N, 15.92°E	75.43°N, 111.80°E	2.43 UT
Longyearbyen EAST (Adventdalen before 2006)	78.19°N, 33.5°E	74.4°N, 123.6°E	3.21 UT
Longyearbyen WEST (Adventdalen before 2006)	78.19°N, -1.7°E	76.9°N, 100.3°E	1.66 UT

A significant limitation of ground based FPIs is that optical measurements of airglow and aurora at thermospheric altitudes are only possible during the night when the sun's zenith angle is greater than 98°. This means that the high latitude FPI observing season runs only in the winter months: from September to April at KEOPS; and October to March at Longyearbyen. The FPIs have been nearly continually observing the 630 nm emission from airglow and aurora every winter night since 1981 and 1986, respectively. Complete 24 hours of observation are possible during November to January at Longyearbyen. Thermospheric winds have been monitored by calculating the Doppler shifts of the 630nm airglow radiation intensities. The FPI instrument has a mirror that rotates to look in several directions (e.g. north, north-east, east, south, west, north-west, zenith and a calibration lamp) to provide line-of-sight wind measurements at a fixed elevation angle. The exposure times can be as low as 10 seconds, up to 120 seconds. A typical complete scan cycle takes ~4 minutes for Kiruna and ~5 mins for Longyearbyen. After 1999, when laser calibrations were made possible, thermospheric temperatures were measured from the thermal broadening of the emission line. More details of operation may be found in Aruliah et al. (2005) and references therein.

The 630nm emission has a peak intensity at an altitude of around 240 km. So measurements of the Doppler shifts and thermal broadening of the emission line are used to determine the winds and neutral temperatures of the upper thermosphere (> 200km altitude). The elevation angle of the mirror is 45° for the Kiruna FPI and 30° for the Longyearbyen FPI. Thus the radius of the field-of-view is 240 km and 416 km, respectively, which represents roughly a 5° and 8° separation in latitude of the north and south viewing volumes at the respective sites. At these high latitudes where the magnetospheric dynamo dominates the plasma flows, ion-neutral coupling can create meso-scale structures in the upper thermosphere on horizontal scale sizes of as little as ~100 km (e.g. Aruliah et al., 2001~~, Emmert et al., 2006a~~). So average wind speeds have been determined for each of the 4 cardinal look directions in order that the meso-scale structure is not lost. The winds are strongly dependent on UT, season, solar cycle and geomagnetic activity due to the dominant forcing mechanisms of pressure gradients and ion-neutral coupling in the high latitude upper thermosphere. The maximum average wind vector magnitudes measured by an FPI at Kiruna were shown to be in the range 100-300 ms^{-1} and the errors of measurements were around 10-20 ms^{-1} (Aruliah et al., 1996). The main sources of error are:

a) ~~Poor~~ poor signal to noise when the 630 nm intensities are low, such as at solar minimum, or geomagnetically quiet conditions.

b) ~~The~~ the existence of large vertical winds. These break the assumption that the winds are predominantly horizontal. Vertical winds are generally small, but can be a few 10s of ms^{-1} at high latitudes (Aruliah and Rees, 1995; Ronksley, 2016). Large vertical winds introduce an error of a few per cent into the calculation of a horizontal wind component from the line-of-sight measurement.

c) The the assumption that the neutral winds are nearly constant with respect to altitude above 200 km owing to the very low density and consequently high molecular viscosity of the upper thermosphere.

The altitude distribution of the 630 nm emission has a peak emission altitude of between 220-250 km (e.g. Link and Cogger, 1988; Vlasov et al., 2005). However, the emission profile also has a full width at half maximum intensity of around 50-70 km, i.e. sampling altitudes tens of km below and above the emission peak. The ground-based FPI observes a height-integration of the emission along the line-of-sight. The measured Doppler shift is therefore an integration of the Doppler shifts at all altitudes, weighted by the emission profile. However, there are several reasons to justify why we are confident that the FPI provides a good sample of the winds at ~240 km altitude. The excited atomic oxygen state in the O (^1D-^3P) transition is a forbidden transition with a long life-time of ~110 sec (Bauer, 1973), which allows the atom to thermalise before emission and be representative of the surrounding gas. Below 200 km the molecular composition increases significantly, and the long lifetime means that the 630 nm emission is quenched due to molecular collisions with N_2 and O_2. Consequently we can assume there is minimal contribution of Doppler shifts from below 200 km altitude, which is a region where the neutral wind magnitude has a large height dependence (note that the horizontal winds at 100 km altitude are a few tens of ms^{-1} while at 250 km altitude are a few hundreds of ms^{-1}). Above the altitude of the emission peak the flux falls off rapidly with altitude and also with distance from the FPI, which minimises the contribution of winds from the region above. Overall it is suggested that the FPI measured winds may underestimate the winds at ~240 km altitude by no more than about 10% due to the contribution of winds below the peak emission height.

4 CMAT2 model winds

The UCL Coupled Middle Atmosphere Thermosphere (CMAT2) model is a 3-dimensional, time-dependent physics-based model, that solves numerically the non-linear coupled continuity equations of mass, momentum and energy (Harris et al., 2002). The model has a latitude resolution of 2°, longitude 18°, and a one third scale height for a height range of ~15 km (top of the troposphere) to 300-600km (top of the thermosphere). Thermospheric heating, photodissociation and photoionisation are calculated for solar X-ray, EUV and UV radiation between 0.1-194 nm (Fuller-Rowell, 1992; Torr et al, 1980a and 1980b; Roble, 1987). High latitude ionospheric parameters of ion and electron densities and temperatures, plus field-aligned plasma velocities, are from the Coupled Sheffield University High-latitude Ionosphere Model (Quegan et al., 1982; Fuller-Rowell et al., 1996). The high latitude auroral precipitation is provided by the TIROS/NOAA auroral precipitation model (Fuller-Rowell and Evans, 1987) and the high latitude electric field model is from Foster et al., (1986). Other features are detailed in Harris et al. (2002). The CMAT2 winds will be presented as part of the discussion below.

5. Results

Data were chosen from the 3-year periods 2001-2003 and 2005-2007, when the CHAMP satellite was in orbit. These represent periods of solar maximum and minimum, respectively. CHAMP data were collected all year around, but the FPI data were limited to nighttime periods only.

5.1 CHAMP average winds

Figures 1 and 2 show plots of average CHAMP accelerometer measurements of the cross-track thermospheric wind component during the whole period of years 2001–2003, that were obtained during direct overflights above the FPI stations at Longyearbyen (Figure 1) and KEOPS (Figure 2). The cross-track wind component is defined as pointing into the positive y-direction of the S/C coordinate system with its x axis along the orbital trace, the z axis toward nadir, and the y-axis completing the right-hand system. The y-wind component therefore points perpendicular to the orbital plane to the right side, when looking in the direction of flight. Given the high inclination (87.3°) of the CHAMP satellite, this corresponds approximately to the geographically eastward direction for the ascending orbital track (blue lines in Figure 1) except for very high geographic latitudes (see below). The cross-track wind measurements of the descending orbital tracks (red lines) have been flipped in sign to get nearly the same eastward wind component.

Figure 1a and 2a show average values for all data, while Figures 1b, 1c, 2b and 2c show the summer and winter averages. There are many more data points for the Longyearbyen station, at a higher geographic latitude compared with KEOPS. This confirms the fact that the relative probability of overhead crossings of high-latitude stations by low Earth orbiting (LEO) satellites with a near-polar circular orbit augments with increasing latitude. A statistical study has to make some compromise with respect to the area of accepted local coincidences of the satellite recordings above the ground-based observations and also with regard to the further data binning. Here, a circular area ~~with~~ based on a 2° latitude radius and hourly bins versus local time have been used which produces a sufficiently good coverage. Further binnings have been been tested to investigate the effect on the results. A shorter radius deteriorates the statistics within the bin, while larger bins tend to smear the spatial and temporal variations. Data filtering with respect to other parameters like, e.g., season, solar wind and interplanetary magnetic field (IMF) values, solar radiation and geomagnetic activity indices should be taken into account if they appear to make a significant effect.

The variance of the cross-track neutral wind magnitude is considerably larger during the whole day above the station at higher latitudes. The average phase of the diurnal eastward wind variation differs also considerably between the data sets of the two observatories. The eastward wind maximizes during the pre-midnight hours over Longyearbyen, while a smaller maximum and a shorter interval of eastward wind is seen at lower latitudes above the KEOPS station (2–3 hours versus about 6 hours). The eastward neutral thermospheric wind is approximately sinusoidal for Longyearbyen (Fig. 1a), but reveals two maxima/minima over the KEOPS station (Fig. 2a). The westward wind maximizes there at about 19 LT and prior to midday (~11 LT). Finally, the variance of the cross-track neutral wind magnitude over the lower latitude station KEOPS is relatively large during the afternoon to early nighttime hours (~15–20 LT). This might be due to the position of this station relative to the large dusk cell which is known to be strongly dependent on, in particular, the IMF By component (cf., e.g., Rees et al., 1986; Killeen et al., 1995; Förster et al., 2008 and Förster et al., 2011). In contrast to

KEOPS, the higher latitude station Longyearbyen is located close to or even poleward of the dusk cell's focus, so that the cross-polar cap circulation of the neutral thermospheric air dominates.

Figure 1: CHAMP observations over Longyearbyen during solar maximum 2001-2003. a) All data – ascending (blue) and descending (red) averages; b) Summer (May-Aug) and c) Winter (end Oct-early Mar).

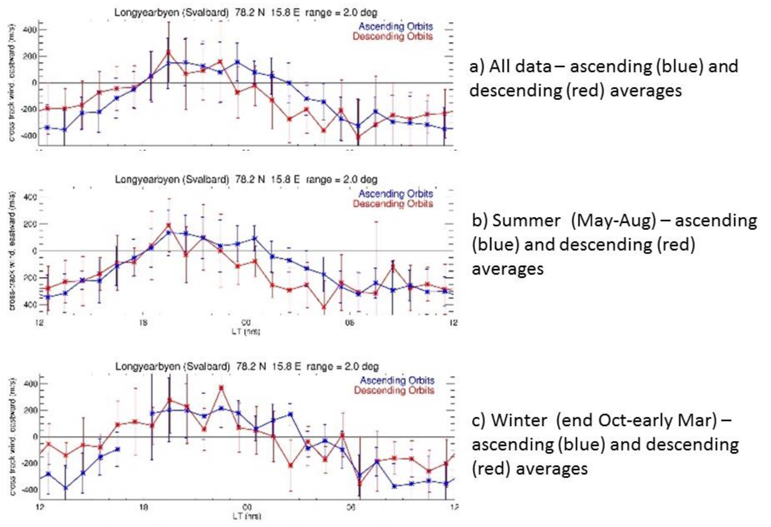

Formatted: Font: Italic

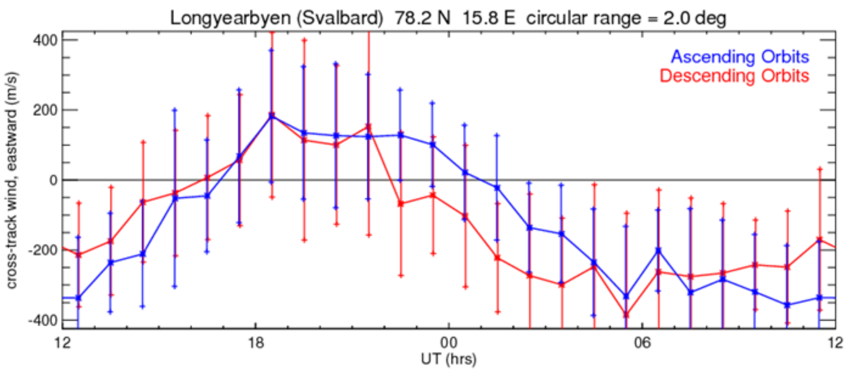

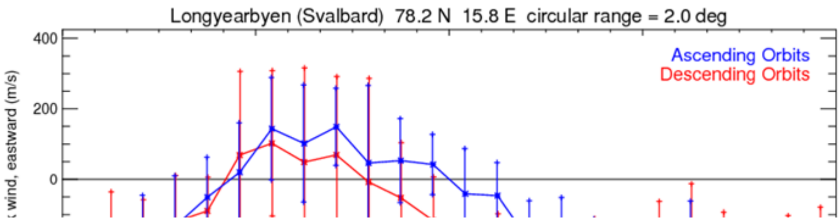

Figure 2: CHAMP observations over KEOPS during solar maximum 2001-2003. a) All data – ascending (blue) and descending (red) averages; b) Summer (May-Aug) and c) Winter (end Oct-early Mar).

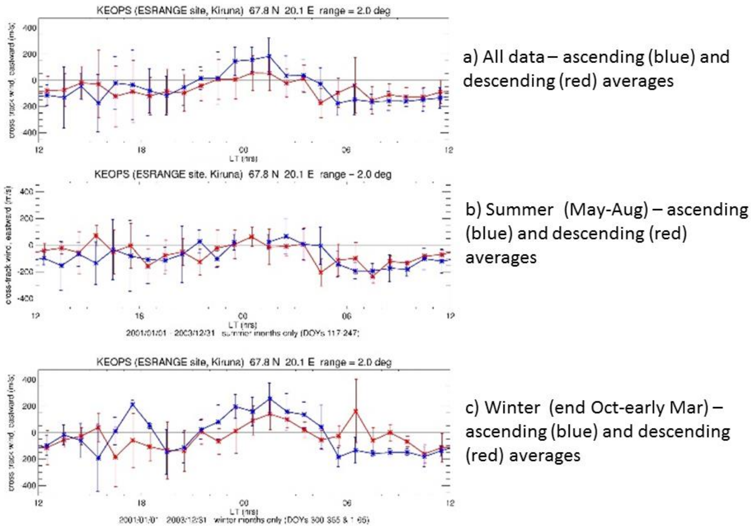

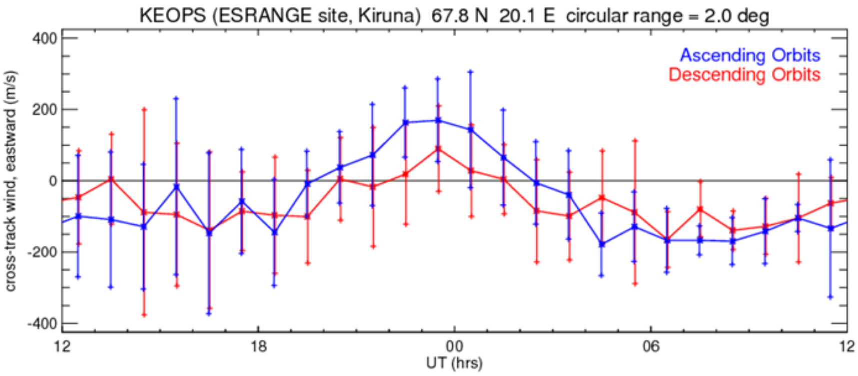

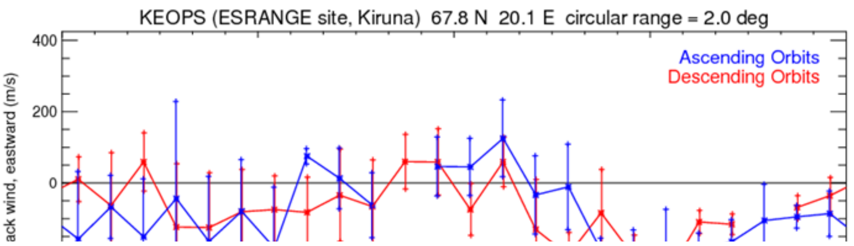

Figures 1b and 1c repeat the statistical plot of Fig. 1a for Longyearbyen for the years 2001-2003 with high solar activity, but confined to the winter and summer months, respectively. Similarly for Figures 2b and 2c for KEOPS. The statistical significance is therefore reduced, in particular for the KEOPS station, but seems to be still sufficient. The winter recordings (Fig. 1c and 2c) during nighttime hours can directly be compared with the FPI observations (Figs. 5 6 and 67).

The principle behaviour of the Longyearbyen and KEOPS eastward wind component is similar to that for the full year coverage, but there are also obvious seasonal differences. The wind component amplitudes, in particular the eastward maxima, are smaller during summer compared with the winter months, while the phases are almost the same. The statements about the variance of the eastward/westward wind component for both stations that have been made with respect to the full year statistics in Fig. 1 hold also for both winter and summer plots, maybe with slightly larger values for the winter months.

The ascending and descending orbits are analyzed separately in their statistical behaviour (blue and red lines and vertical bars, respectively), and show distinct differences. This points to the problem of co-alignment of the ascending and descending orbital tracks (despite the simple sign flip). The small offset of ~2.7° from a strict polar orbit of the satellite causes some deviation from the east/westward pointing of the cross-track measurements. At low to mid-latitudes, the deviation from purely geographically eastward direction corresponds in good approximation to this colatitude angle of the satellite's inclination $\beta \approx 2.7°$, but at high latitudes and in particular near the poles it can deviate considerably. This non-alignment angle α (deviation from purely eastward) can be estimated in dependence on the observer's colatitude θ with spherical angle relations using a simplified spheric geometry of the Earth as in Eq. (14).

$$\alpha = \arcsin\left(\frac{\sin\beta}{\sin\theta}\right) \qquad (14)$$

Using the geographic coordinates of the observatories in Table 1, one gets an α-angle of 7.2° and 13.3° for KEOPS and Longyearbyen, respectively. The angular difference ($2 \cdot \alpha$) between the two one-component cross-track wind measurements of the ascending and descending orbital tracks is already considerable for the most northward station at Longyearbyen and this offset can be noticed in, for example, Figure 1a as an offset between the wind averages for ascending and descending orbital tracks during certain intervals, where the wind component perpendicular to the zonal wind direction, i.e. the north-south meridional wind, is large. This is obviously the case for the nighttime hours between 23–05 LT and the daytime hours between ~10–17 LT for Longyearbyen and for a few nighttime hours between 23–03 LT for the KEOPS FPI station.

If the FPI technique, in particular the tri-static measurements for certain periods (Aruliah et al.,2005; Griffin et al., 2008), allows the determination of specified neutral wind directions, one might consider comparing the wind magnitudes for the descending and ascending orbital tracks separately for an eastward $\pm\alpha$ orientation, respectively. Here, one should note, that at an observation point with an even higher geographic latitude (ideally at ~86.2° geographic latitude, where the two branches of one-component observations would be perpendicular to each other) it would in principle be possible to derive the full thermospheric horizontal wind vector from the cross-track accelerometer measurements. This is, strictly spoken, valid in a statistical mean with characteristic times of a few days, i.e. with the repetition period of ascending and descending orbits over one and the same high-latitude location.

The meridional component is much larger than the zonal one during considerable periods of the nighttime observation. So, to minimize the error in comparing the neutral wind magnitude, it would be better to compare the full vectors. Already a small error of the measurement orientation could make a large effect on the relatively small eastward wind component, which could lead us to wrong conclusions about the characteristics of the differences between FPI and CHAMP accelerometer measurements. The offset between the geographic and geomagnetic coordinates allows the construction of the full horizontal vector plots as statistical averages taken over a period of at least 131 days of CHAMP's precession period in order to cover all local times. This statistical mapping is limited to magnetic latitudes poleward of about > 60° for both hemispheres (cf. Förster et al., 2008).

Figure 3: Geometry illustrating the projection of FPI look direction horizontal wind components onto the CHAMP cross-track direction for the ascending and descending tracks.

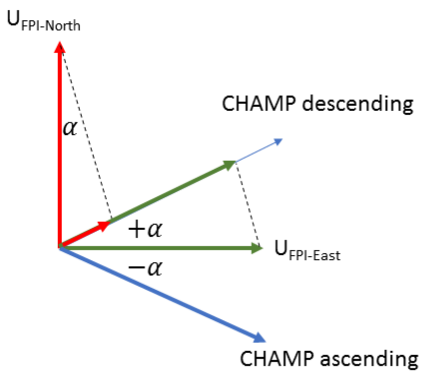

Figure 3 illustrates the projection of the horizontal wind component from the north and east FPI look directions onto the cross-track direction of the CHAMP ascending direction. It also illustrates how the average of the CHAMP ascending and descending winds gives the zonal wind component. The projections of the FPI wind vectors onto each of the ascending and descending directions are used later in determining the ratio of the CHAMP/FPI wind magnitudes (see section 5.2 Figure 10).

Formatted: Font: Not Italic

Figure 43: CHAMP observations over Longyearbyen during solar minimum 2005-2007. a) All data – ascending (blue) and descending (red) averages; b) Summer (May-Aug) and c) Winter (end Oct-early Mar).

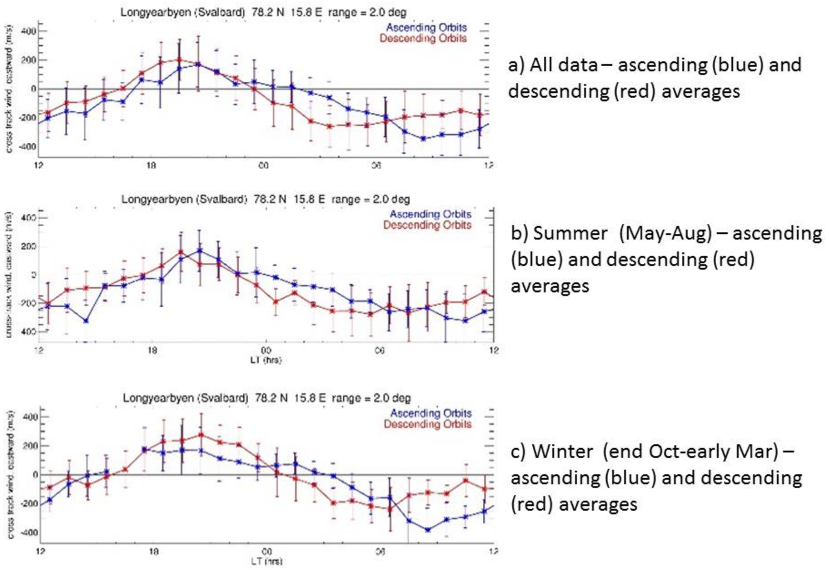

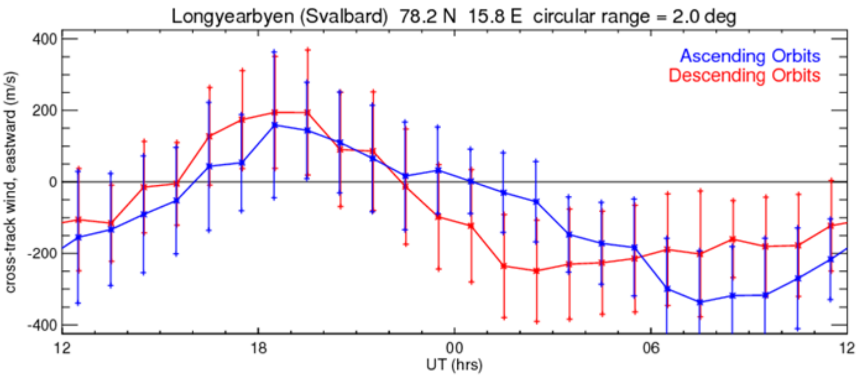

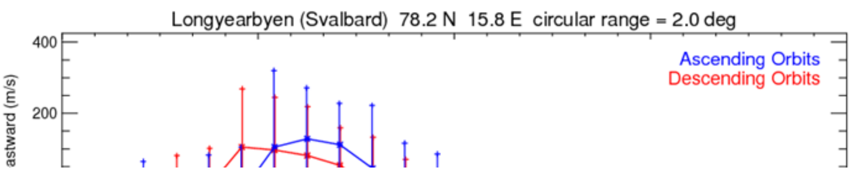

Figure 54: CHAMP observations over KEOPS during solar minimum 2005-2007. a) All data – ascending (blue) and descending (red) averages; b) Summer (May-Aug) and c) Winter (end Oct-early Mar).

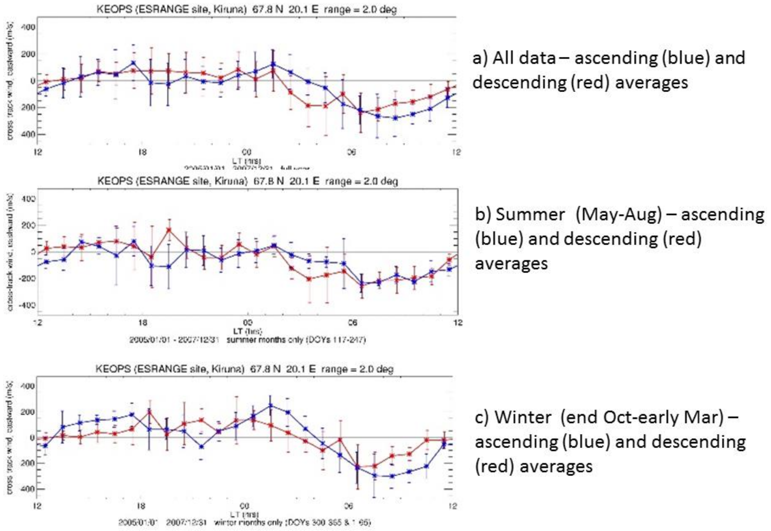

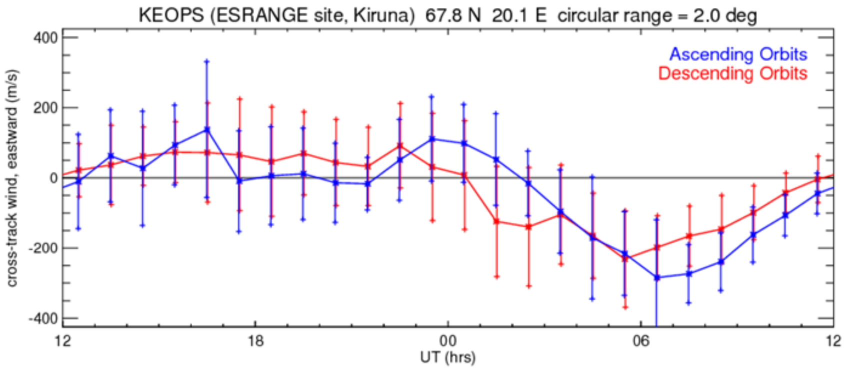

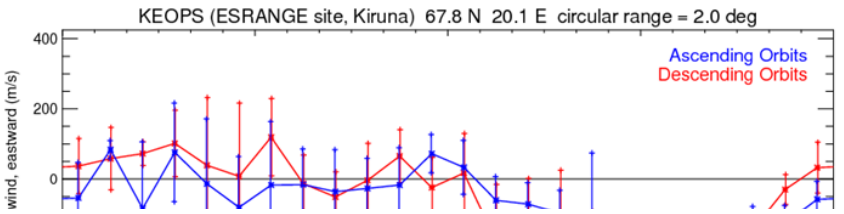

Figures ~~3~~ 4 and ~~4~~ 5 show the corresponding plots to Figs. 1 and 2, but now for low solar activity conditions during the years 2005-2007. They reveal some differences as, e.g., generally smaller amplitudes and different wind phases. Here, the zonal wind above KEOPS seems to point eastward during most times of the day except the morning hours 04–11 LT.

5.2 FPI average winds

The average winds observed at Kiruna and Longyearbyen are presented in Figures ~~5~~ 6 and ~~6~~7. Local Time is 1 hour ahead of Universal Time for both sites. The format of these figures is that the plots ~~5a~~6a, ~~5c~~6c, ~~6a~~ 7a and ~~6c~~ 7c show the average zonal wind component, comparing observations from the volumes to the East and West of the site. The plots ~~5b~~6b, ~~5d~~6d, ~~6b~~ 7b and ~~6d~~ 7d show the average meridional wind component from the volumes observed to the North and South ~~look directions~~. The full set of cardinal direction measurements, are presented to provide a context for the comparison with the zonal wind measurements made by CHAMP, especially since the CHAMP y-axis is only roughly zonal. The standard error of the mean ε is added as an error bar to the FPI East and North data, where $\varepsilon = \sigma/\sqrt{(N\text{-}1)}$, σ is the standard deviation and N is the number of data points. The standard errors of the mean (rather than the standard deviations) demonstrate the distinctly different trends in the winds observed in the volumes to the East and West of the sites, i.e. the meso-scale structure of the high-latitude thermosphere.

The periods of data cover the winter months of 2001-2003 and 2005-2007 to match with the CHAMP datasets. The FPIs cannot measure winds during cloudy periods owing to the scatter of light by the clouds, and are only able to observe the emission during the hours of darkness. Thus the observing days cannot be identical to the dates when CHAMP passed overhead of the two sites. Longyearbyen has 24 hours of darkness during the months of November to January, so there are nearly 24 hours of observations, but the longest period of darkness at Kiruna is around 18 hours in mid-winter. CHAMP, meanwhile, is able to provide a full 24 hours of observations from drag measurements.

There are consistent differences in the winds observed to the geographic East and West, or to the North and South. This is understandable because the Kiruna site is, on average, at the equatorward edge of the auroral oval, while Longyearbyen is mostly in the polar cap, though ~~at~~ towards the poleward edge of the auroral oval. The expansion and contraction of the auroral oval during an active period means that the northern half of the FPI field-of-view can be very different from the southern half. In fact, Emmert et al. (2006~~b~~) have shown that high latitude neutral winds are better ordered in geomagnetic coordinates of magnetic latitude and magnetic local time than in geographic coordinates and universal time. The AACGM geomagnetic coordinates shown in Tables 1 and 2 give an indication of how different are the magnetic latitudes for the East and West look directions.

Figure ~~5~~ 6 shows average zonal and meridional winds from FPI observations at Longyearbyen. Figs ~~5a~~ 6a and ~~5b~~ 6b show solar maximum years (2001-2003), while Figs ~~5c~~ 6c and ~~5d~~ 6d show solar minimum years (2005-2007). Figs ~~5a~~ 6a and ~~5c~~ 6c show the zonal winds to the East and West using the convention of +East, while Figure ~~5b~~ 6b and ~~5d~~ 6d shows the meridional winds to the North and South, using +North. The average standard deviations σ are ±103 ms^{-1} and ±64 ms^{-1} for the solar maximum zonal and meridional winds, respectively

Formatted: Superscript

Formatted: Superscript

Formatted: Tab stops: 1.27 cm, List tab

Figs 56 a and b show solar maximum (2001-2003) FPI winter average wind components at Longyearbyen for geomagnetically quiet conditions (0 ≤ Kp < 2-). a) Zonal and b) meridional average winds and the standard errors of the mean are plotted. North and East are purple lines, while South and West are light blueFig 5 FPI winter average wind components at Longyearbyen for geomagnetically quiet conditions (0<Kp<2). The standard error of the mean is

Formatted: Don't adjust space between Latin and Asian text, Don't adjust space between Asian text and numbers

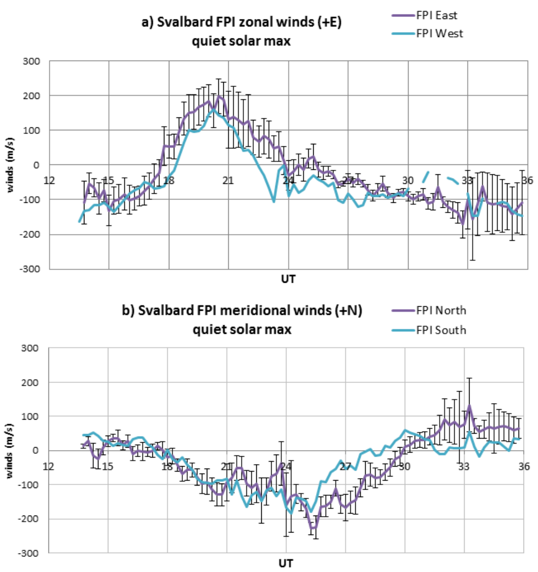

Fig 5 FPI winter average wind components at Longyearbyen for geomagnetically quiet conditions (0<Kp<2). The standard error of the mean is shown for one example component.

Solar maximum (2001-2003)

a) Zonal average winds
b) Meridional average winds

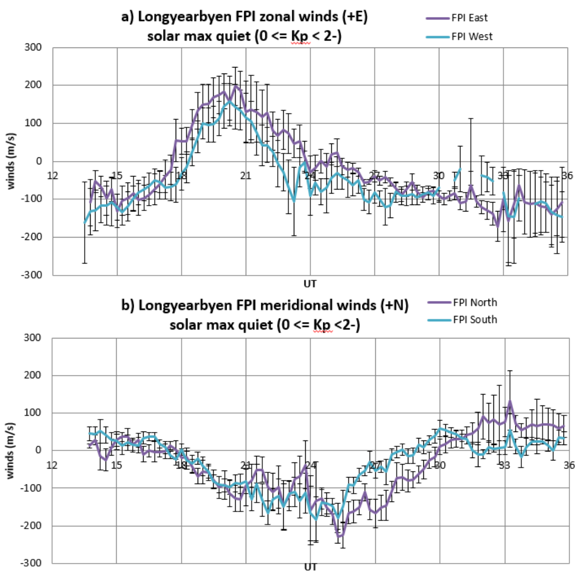

~~shown for one example component. Solar maximum (2001-2003) a) zonal, b) meridional average winds. Solar minimum (2005-2007) c) zonal, d) meridional average winds. North and East are purple lines, while South and West are light blue.~~

Formatted: Font: 10 pt, Not Bold, Italic

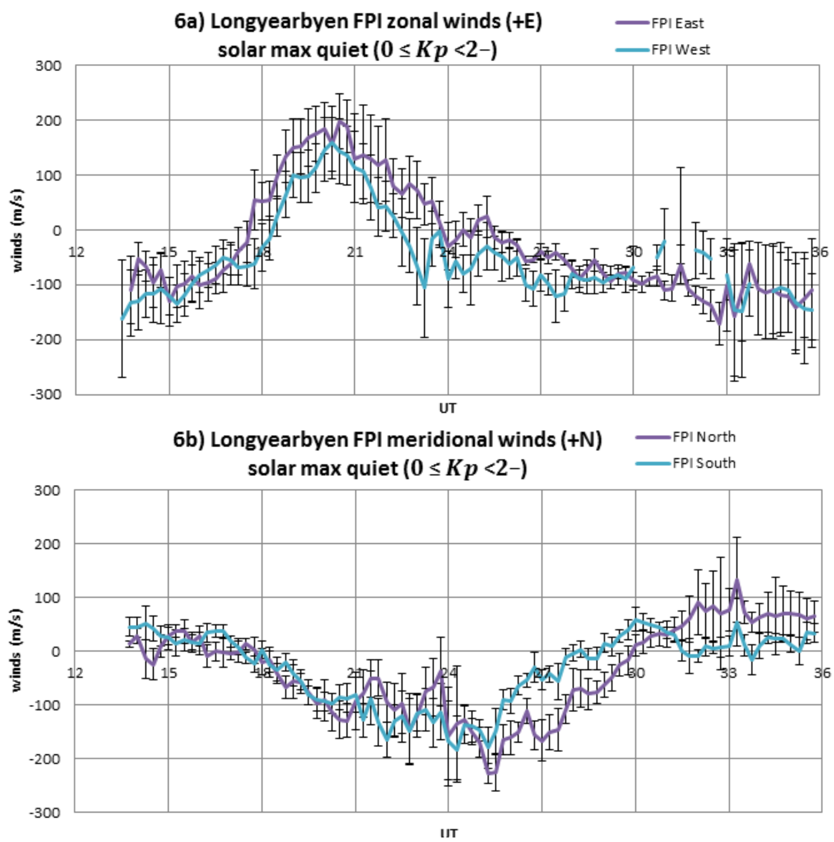

Fig 56 c and d show solar minimum (2005-2007) FPI winter average wind components at Longyearbyen for geomagnetically quiet conditions ($0 \leq Kp < 2-$). a) Zonal and b) meridional average winds and the standard errors of the mean are plotted. North and East are purple lines, while South and West are light blue.Fig 5 FPI winter average wind components at Longyearbyen for geomagnetically quiet conditions ($0<Kp<2$). The standard error of the mean is shown for one example component. Solar maximum (2001-2003) a) zonal, b) meridional average winds. Solar

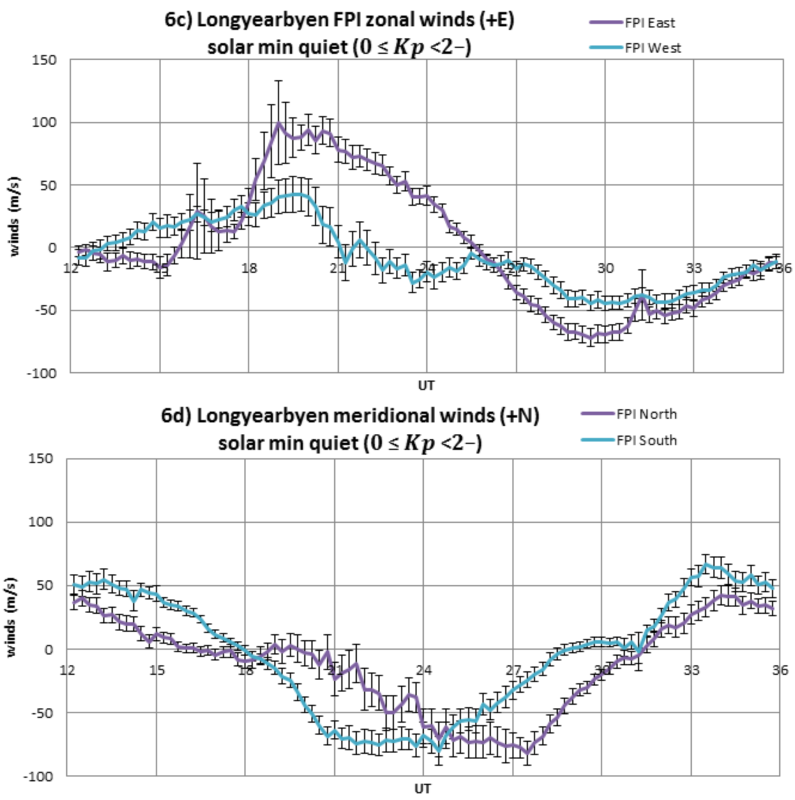

minimum (2005-2007) c) zonal, d) meridional average winds. North and East are purple lines, while South and West are light blue.

Longyearbyen is just within the polar cap. The winds are predominantly antisunward despite the geomagnetic activity level, since this is the direction for both the pressure gradient and ionospheric convection. As a result, Longyearbyen observations are a somewhat less obvious indicator of ion-neutral coupling behaviour than observations at KEOPS in the period 1800-2100 UT. The Longyearbyen solar maximum (2001-2003) winter winds (day numbers 300-65), during geomagnetically quiet conditions (0 ≤ Kp < ~~2o~~2-) are shown in Figures ~~5a~~ 6a and ~~5b~~6b. The zonal winds (Figure ~~5a~~6a) show westward winds before 1800 UT and then eastward winds for ~6 hours which then turn westward. The maximum wind speed is about 200 ms^{-1} eastward between 1800-2400 UT. The meridional winds (Figure ~~5b~~6b) are slightly northward before 1700 UT, then turn southward until 0600 UT, and return northward. The maximum speed is about 200 ms^{-1} southward at about 0100 UT. The standard errors of the mean are around ±30 ms^{-1}, however the values vary systematically through the night. Between 1800-2100 UT the standard error is around 3 times larger than between 0300-0900 UT when it is very small.

Figures ~~5c~~ 6c and ~~5d~~ 6d show the Longyearbyen FPI winds for clear nights during winter (DOY 300-65) 2005-2007, geomagnetically quiet conditions (0 ≤ Kp < ~~2o~~2-). There is a full 24 hours of observations in this dataset, and the extreme quiet of this solar minimum period has provided a large number of observations for this category. The antisunward flow appears clearly. There is a strong phase lag between the observations to the North and South. This is puzzling because it cannot be explained in terms of ordering high latitude winds in geomagnetic coordinates. This category is for the most geomagnetically quiet conditions possible: solar minimum during a prolonged solar minimum, and the lowest Kp values. Under these conditions the geographic coordinate system under which the solar flux heating operates, should be the most appropriate. The average standard deviations are ±55 ms^{-1} and ±47 ms^{-1} for the zonal and meridional winds, respectively. The standard errors of the mean are very small, ~~around~~ averaging less than ±10 ms^{-1}, though again there is a clear systematic UT-dependent trend. Between 2100-0300 UT the standard error of the meridional wind is about 2-3 times larger than at other times. Between 1500-2000 UT the zonal wind standard error becomes considerably larger.

Fig ~~7~~6 ~~a and b show solar maximum (2001-2003) FPI winter average wind components at KEOPS for geomagnetically quiet conditions (0 ≤ Kp < 2o). a) Zonal and b) meridional average winds and the standard errors of the mean are plotted. North and East are purple lines, while South and West are light blue.~~

~~Fig 6 FPI winter average wind components at KEOPS for geomagnetically quiet conditions (0<Kp<2). The standard~~

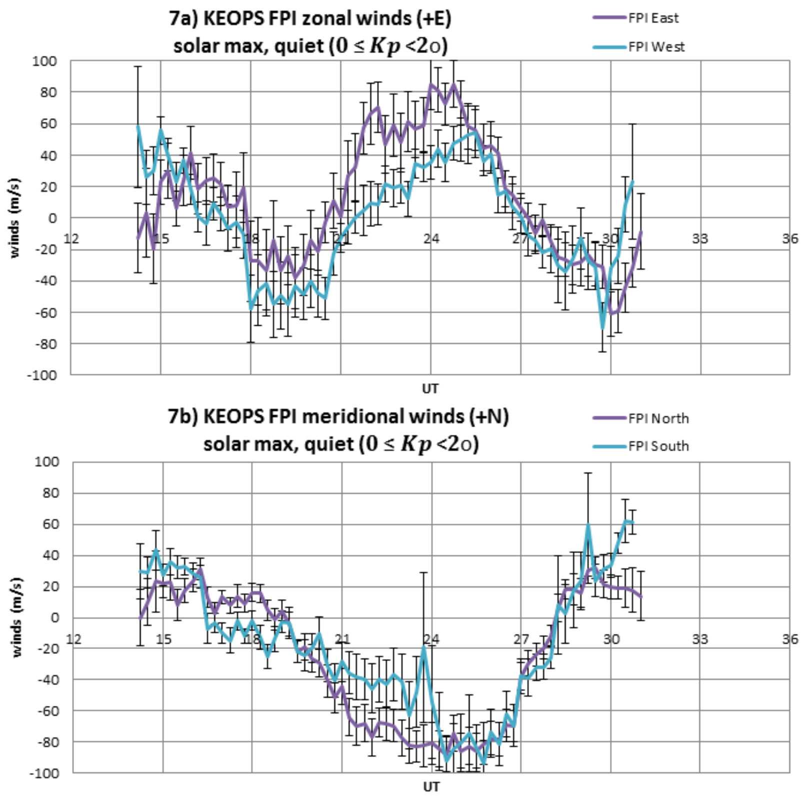

~~error of the mean is shown for one example component. Solar maximum (2001-2003) a) zonal, b) meridional average winds. Solar minimum (2005-2007) c) zonal, d) meridional average winds. North and East are purple lines, while South and West are light blue.~~

Fig 57 c and d show solar minimum (2005-2007) FPI winter average wind components at KEOPS for geomagnetically quiet conditions (0 ≤ Kp < 2-). a) Zonal and b) meridional average winds and the standard errors of the mean are plotted. North and East are purple lines, while South and West are light blue.~~Fig 6 FPI winter average wind components at KEOPS for geomagnetically quiet conditions (0<Kp<2). The standard error of the mean is shown for~~

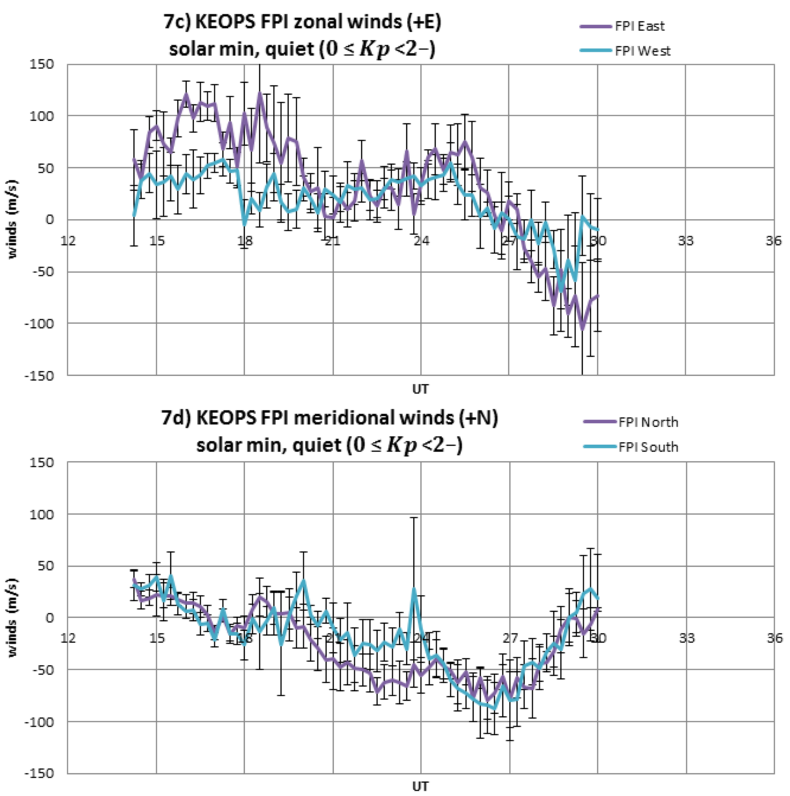

~~one example component. Solar maximum (2001-2003) a) zonal, b) meridional average winds. Solar minimum (2005-2007) c) zonal, d) meridional average winds. North and East are purple lines, while South and West are light blue.~~

Formatted: Font: Not Italic

Figure 76 shows the KEOPS FPI winds for clear nights during winter (DOY 300-65) ~~geomagnetically quiet~~~~moderately active~~during geomagnetically quiet conditions. ~~(0 ≤ Kp < 2o).~~ The general diurnal trends are similar for both solar maximum (Figs ~~6a~~7a, b) and minimum (Figs ~~6c~~7c, d). The solar minimum data range is 0 ≤ Kp < 2-, but i~~I~~t was necessary to increase the geomagnetic activity spread for the solar maximum data to improve the statistics, so Figures 7~~6~~a, b show ~~(~~0 ≤ Kp < 2o~~)~~. The meridional winds show antisunward flow that is predominantly driven by the pressure gradient from dayside EUV heating, resulting in fairly weak southward winds reaching a maximum value of nearly 100 ms^{-1}. The standard errors of the mean are around ±10-15 ms^{-1}. The zonal winds are eastward before 1800UT, reaching a maximum speed of a few 10s ms^{-1}. After 1800 UT the zonal winds turn westward for a few hours and back eastwards around 2100UT. Between 2100-0300 UT the zonal winds reach their maximum speed of up to 80 ms^{-1} before turning westward again. The zonal winds are more variable, and their standard errors of the mean are slightly larger than for the meridional winds, at around ±20 averaging 1630 ms^{-1}.

The few hours of westward flowing zonal winds during 1800-2100 UT are particularly interesting (Figs 6a 7a and 6c7c). The westward flow indicates that the winds are briefly under the influence of the clockwise dusk cell of ionospheric convection. Through collisions between the ions and neutral gas, momentum is transferred to the neutrals, which diverts them from the direction of the pressure gradient driven anti-sunward/eastward flow. The action of the centrifugal force balancing the Coriolis force keeps the winds entrained in the cell (Fuller-Rowell and Rees, 1984). As the KEOPS site passes under the region of the Harang Discontinuity (Harang, 1946), the FPI West zonal winds turn back to eastward about 40 mins after the FPI East zonal winds. This is because the KEOPS FPI East observing volume is a horizontal distance of 480 km away from the FPI West volume (note that the distance between the viewing volumes depends on the altitude of the 630 nm emission). However, note that at the latitude of KEOPS, the time taken for the Earth to rotate through a distance of 480 km is 46 mins. The difference between 40 min and 46 min is partly due to the difference in magnetic latitude. It is also due to the Harang Discontinuity being dependent on the IMF B_y orientation, resulting in a smearing out of the MLT interval.

Figures 6c 7c and 6d 7d show the KEOPS FPI winds for clear nights for the years 2005-2007 during winter (day numbers 300-65), geomagnetically quiet conditions ($0 \leq Kp < 2o2-$). These years were during the unusually extended solar minimum of the last solar cycle when the solar flux levels were extremely low, and observations of aurora were rare. Consequently the plasma density was smaller, and the thermosphere was more compressed, resulting in smaller neutral densities at a given height. Under these conditions the ion drag driver is less efficient, and the pressure gradients, together with the Coriolis and centrifugal forces, play a larger role. Thus, although the trends are similar to the solar maximum winds; the zonal winds are strongly eastward throughout the evening sector. There are no westward zonal winds until after 0300 UT, and generally the wind amplitudes are smaller. The maximum meridional wind is about 80 ms^{-1} southward around 0300 UT. The maximum zonal winds are seen to the East, and these are around 100 ms^{-1} eastward in the evening sector and start to increase westwards towards 100 ms^{-1} by 0600 UT. The average standard errors of the mean are around ± 230 ms^{-1}, which are larger than for solar maximum conditions.

The general trends seen in the northern winter geomagnetically quiet CHAMP zonal winds (Figures 1-2, and 4-5) are also seen in the FPI winds (Figures 6-7). The phases match extremely well for both sites, h(a) Longyearbyen and (b) KEOPS. However, there is a considerable difference in magnitude. The next 2two figures (Figures 8-9) show direct comparisons of CHAMP and FPI winds along the cross-track direction for moderately active conditions ($2^- \leq Kp < 4^+$). There is a lot of modelling effort into studying the active ionosphere-thermosphere, which makes this comparison useful. In particular it is relevant to the argument in section 6.4

Formatted: Adjust space between Latin and Asian text, Adjust space between Asian text and numbers

Formatted: Font: (Default) Times New Roman

Formatted: Font: (Default) Times New Roman

where CHAMP and FPI neutral winds are compared with typical ion velocities actively observed by ground-based radars at high latitudes.

.The average ratio of the zonal wind magnitudes (CHAMP /FPI) for Longyearbyen is 1.8, and for KEOPS is 3.3.

Fig 8 Longyearbyen (Svalbard) winters 2001-20034, $2^- \le$ <Kp $< 4^+$: average zonal winds measured using CHAMP and FPI, including standard errors of the mean. These are compared with FPI winds observed by the University of Alaska in 1980, and the HWM93 model winds. Fig 7 Longyearbyen (Svalbard) winters 2001-2004, 2<Kp<4: average

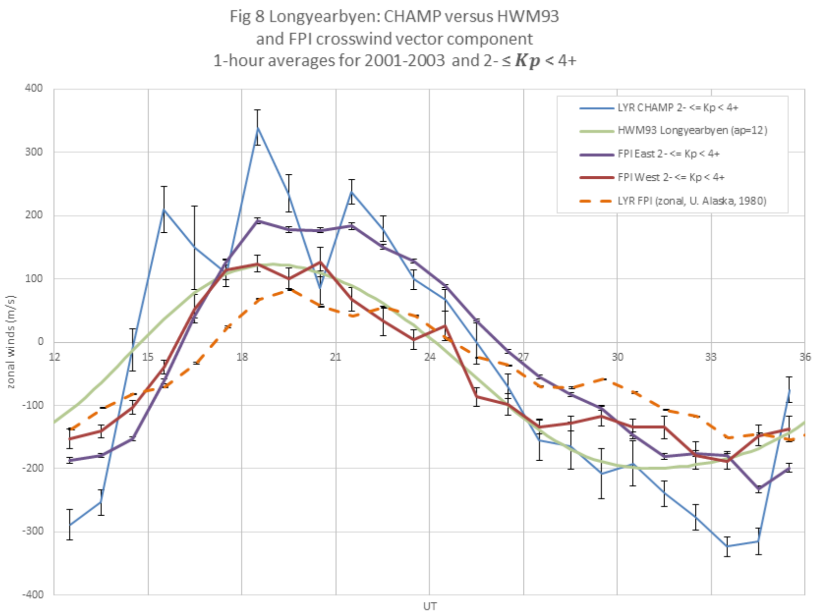

zonal winds measured using CHAMP and FPI, including standard errors of the mean. These are compared with FPI winds in 1980 and the HWM87 and HWM90 model winds from Hedin et al (1991).

Figure 87 is a direct comparison between CHAMP cross-track winds at Longyearbyen from and several different sources. The winds represent moderately active conditions ($2^- \le$ Kp $< 4^+$) during winter months (November to JanuaryDOY 300-65) for solar maximum years. The HMW93 model is setconditions are for the 31st December atwith ap = 12 (Kp = 3-); F10.7 =150; height 400 km (Hedin et al., 1996). At Longyearbyen there iscan be 24--hour coverage by the FPI owing to continual darkness between November-January. The of Longyearbyen zonal windsdirect comparison is made by projecting t.he components of the FPI and HMW93 (Hedin et al., 1996) wind vectors along the CHAMP ascending and descending cross-track directions using the appropriate values of ± $\alpha = \pm 13.3°$ for the two sites. These represent moderately active conditions (2^- < Kp <

Formatted: Font: (Default) Times New Roman
Formatted: Font: (Default) Times New Roman
Formatted: Font: (Default) Times New Roman
Formatted: Font: Italic
Formatted: Adjust space between Latin and Asian text, Adjust space between Asian text and numbers
Formatted: Font: Not Italic
Formatted: Font: Calibri, 9 pt, Do not check spelling or grammar
Formatted: Font: Not Italic
Formatted: Superscript
Formatted: Superscript

~~4⁻) during winter months (November to January) for solar maximum years that are 20 years apart.~~ CHAMP cross-track winds ~~were collected during the years 2001-2004, while the~~and UCL Longyearbyen FPI observations ~~were~~ are averages for ~~during~~ 2001-2003 (a failure occurred in the rotating mirror mechanism in late December 2003 so CHAMP 2004 data were not included). The ~~CHAMP~~ data are then the averages of the ascending and descending ~~orbits~~components to give a zonal wind.

FPI wind v~~V~~alues taken from Figure 9 in the paper by Hedin et al. (1991) are also plotted. These values are measurements from the University of Alaska FPI that collected Longyearbyen data in 1980, 1981 and 1983.~~;~~ The aim is to demonstrate that the FPI technique of measuring Doppler shifts gives consistent results, which is discussed in section 6.2. ~~and the HWM87 and HWM90 model.~~ The U.Alaska FPI winds ~~are~~ were an average of the East and West look directions, justified by the assumption of a uniform horizontal wind field over the field of view. This was a common practice at that time owing to a) the assumption of a large molecular viscosity of the thermosphere which reduces wind shear, and b) the longer exposure times of the earlier FPIs (6-12 minutes) which used photomultipliers with piezoelectrical scanning of the FPI etalon gap size in order to view the full Free Spectral Range (Deehr et al., 1980). ~~For Figure 7, only the UCL Longyearbyen FPI East direction winds are shown (Figure 8a shows both East and West look directions).~~ The UCL FPIs were amongst the first FPIs to use fixed gap etalons to image the full FSR onto a 2D array of pixels. This allowed shorter exposure times, and a rapid cycle of look directions, which consequently revealed mesoscale spatial and temporal structures of the order of a few 100 km horizontally and minutes (e.g. Aruliah and Griffin, 2001, Aruliah et al, 2005). During the 1980s and 1990s we used state-of-the-art UCL designed and built Imaging Photon Detectors (McWhirter et al., ~~1981~~1982). Astrocam Antares cameras replaced the IPD in the Svalbard FPI ~~in~~from 1998, and in the KEOPS 630 nm FPI in 2002. However, these cameras had the disadvantage of slow readout times which were essential for the best noise performance and so time resolution was compromised. In 2003 the first Electron Multiplying CCDs revolutionised low light level imaging. These cameras combined superior signal to noise ratio with very fast readout times. The first one was put into service at KEOPS in 2003, followed by Svalbard in 2005 ~~and then EMCCDs (Andor iXon 887/885) were installed around 2005~~ (McWhirter, 2008). The ~~revolution~~ huge advancement over the last 30 years in low light detectors has allowed atmospheric gravity wave observations ~~with~~ using exposure times as little as 10 seconds at auroral latitudes (Ford et al., 2007). Note that t~~T~~he upgrade of the detector is to improve the photon sensitivity which reduces the error of measurement. It does not change the calibration of the wind speeds.

Any changes of etalon required re-calibration of the measured Doppler shift to calculate wind ~~scalculation~~, as discussed in section 6.2. The KEOPS FPI used a 10 mm etalon gap up to January 2002, when it was replaced with an 18.5 mm gap etalon. Then in January 2003 a 14 mm etalon was put in, which has been there until the present time. For the Longyearbyen FPI there was a 14 mm etalon until April 2005, which was replaced with an 18.5 mm etalon from September 2005 until the present time.

All sources show generally similar phases, with peak eastward winds in the evening sector, between 18-24UT and westward winds in the morning sector, between 06-12UT, as expected for anti-sunward flows. Table 2 shows that the AACGM MLT for Longyearbyen is about 2.4 (± 0.8 for the East and West volumes) hours ahead, so magnetic midnight is approximately at 21.6 UT. The standard errors of the mean are plotted for all

Formatted: Superscript

Formatted: Font: Not Bold

Formatted: Font: Not Bold

Formatted: Font: Not Bold

Formatted: Font: Not Bold

Formatted: Font: Not Bold

Formatted: Font: Not Bold

Formatted: Font: (Default) Times New Roman

Formatted: Font: (Default) Times New Roman

Formatted: Font: (Default) Times New Roman

Formatted: Font: (Default) Times New Roman

Formatted

Formatted: Don't add space between paragraphs of the same style, Line spacing: Multiple 1.15 li data. The U.Alaska Longyearbyen FPI standard deviations are around ± 150 ms^{-1}, which are similar to the UCL FPI. For the purposes of comparison, a standard error of ± 30 ms^{-1} is plotted for the U.Alaska FPI data, similar to the average UCL FPI standard error. It was noted in the Hedin et al (1991) paper that for both hemispheres, the average high latitude winds from the FPIs at Sondrestrom, Longyearbyen and College in the northern hemisphere, and Mawson in the southern hemisphere, showed a systematically smaller diurnal variation than the DE 2 mass spectrometer data. The HWM87 model was based on satellite data from the DE 2 and AE-E satellites. Consequently, the addition of the FPI and incoherent scatter radar datasets to the HWM90 database resulted in a smaller diurnal variation compared with the HWM87 winds. The more recent measurements from CHAMP and the UCL FPI are clearly systematically typically different in magnitude, but consistent with the trend noticed by Hedin et al (1991) for satellite wind measurements to be larger than from ground-based FPIs. The diurnal amplitude of the UCL zonal winds is about 170 ms^{-1}, and for the U.Alaska winds is about 125 ms^{-1}. The CHAMP zonal winds are systematically the largest in magnitude, with a diurnal amplitude of around 300 ms^{-1}.

The average of the monthly F10.7 fluxes is 193 184 for the winter periods Nov-Jan Feb of 1980-81, 1981-82 and 1983-84, and 170 160 for the winters of 2001-2003. Yet despite the higher average solar flux in 1980, the UCL FPI zonal wind magnitudes have a significantly larger amplitude than the U.Alaska zonal winds. Closer inspection of the 3 winter periods of 2001-2003 shows a spike in the average monthly F10.7 for November 2001-January February 2002 (i.e. <F10.7> is 168 214 for Nov-Jan Feb 2001-2002; 219 145 for Nov-Jan Feb 2002-2003; and 152 123 for Nov-Dec 2003) which may account for the 3 winter average UCL FPI winds being larger than for U.Alaska. The geomagnetic activity levels are similar, averaging Kp values in the range 3^- to 3^o for all three winters. These are interannual and inter-solar cycle discussions for a later paper.

Formatted: Superscript

Formatted: Superscript

Fig 9 Comparison of CHAMP and FPI measurements of KEOPS zonal average winds to the FPI East and West volumes, including standard errors of the mean, for winters 2001-20043. These are compared the HWM93 model

Formatted: Font: Not Italic

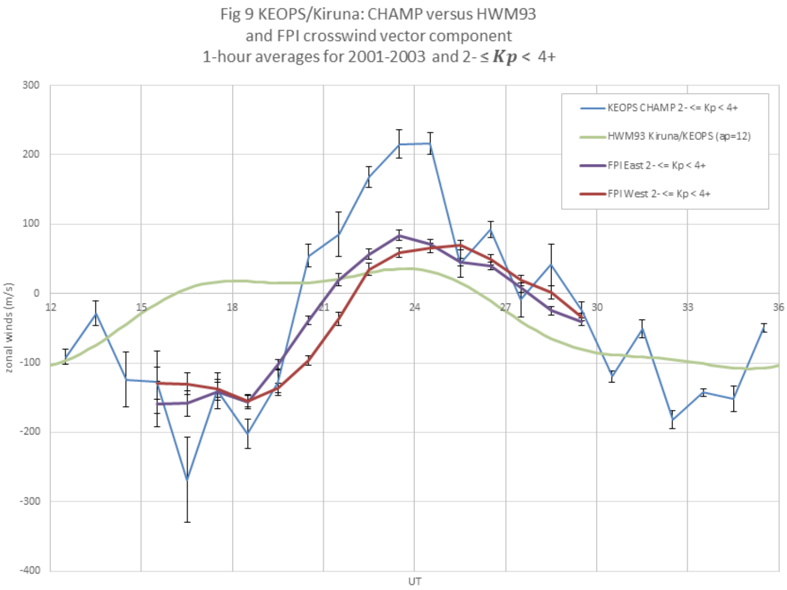

winds.

~~**Fig 8a Comparison of CHAMP and FPI measurements of Longyearbyen (Svalbard) zonal average winds, including standard errors of the mean, for winters 2001-2004. Plus comparison with Alaska 1980 from Hedin et al. (1991). Fig 8b Comparison of CHAMP and FPI measurements of KEOPS zonal average winds, including standard errors of the mean, for winters 2001-2004.**~~

Figure ~~8a and 8b~~9~~8~~ shows a comparison of the CHAMP zonal winds against the UCL FPI winds at Kiruna/KEOPS for the solar maximum winters of 2001-~~2004~~2003. ~~. At Longyearbyen there is 24 hour coverage by the FPI owing to continual darkness between November-January (Figure 8a).~~ The FPI and CHAMP data are selected for moderately active conditions (2^- ≤ ~~<~~ Kp < 4^+) as in Figure 8~~7~~. ~~Here the UCL FPI West look direction is added. Also plotted are CHAMP data for all activity levels. The Alaska average of East and West look directions from 1980-1983 completes the plot. Overall there is a very close agreement in phase between the CHAMP and FPI zonal winds. However, there is a noticeable difference between the UCL FPI East and West look directions. Table 2 shows that the AACGM magnetic latitude of Longyearbyen West volume is nearly 2° further poleward than the East volume, which results in weaker emissions and larger error bars. In addition there is a small phase shift owing to the different magnetic coordinates as discussed further in the next paragraph.~~

At Kiruna the hours of darkness are between 15-06UT for the period November-January. The direct comparison is made by taking the component of FPI and HMW93 (Hedin et al., 1996) wind vectors in the CHAMP cross-track direction using $\alpha = \pm 7.2°$. T~~T~~he UCL FPI average zonal winds for 2- ≤ ~~<~~ Kp < 4+ are shown separately for the East and West look directions~~ in Figure 8b~~. There is a smaller difference between these look directions than for the Longyearbyen zonal winds. The evening winds for moderately active solar maximum conditions are around -150 ms^{-1} (westward), and reach a peak of around 70 ms^{-1} (eastward) in the midnight sector. The AACGM MLT for Kiruna is about 1.9 (± 0.3 for the East and West volumes) hours ahead, so magnetic midnight is approximately at 22.1 UT, which is the time separating the period of the evening eastward electrojet and the morning westward electrojet in magnetic local time coordinates. The behaviour of the zonal winds shows strong ion-neutral coupling for these moderately active conditions, so that there is a semidiurnal variation representative of the twin cell ionospheric convection pattern at auroral latitudes. This is in addition to the day-night diurnal variation of winds driven by the pressure gradient.

The phase of the CHAMP zonal winds is in good agreement, but the amplitude is considerably larger. The peak evening wind reaches -200 ms^{-1} (westward) and 200 ms^{-1} (eastward) by 02 UT. What is particularly interesting about this comparison is the difference between the CHAMP and FPI winds in the period 15-20 UT. The CHAMP winds are considerably less westward, and are more similar to FPI average zonal winds for geomagnetically quieter conditions at solar maximum, as shown in Figure 7~~6~~a. The large standard error of the mean during the period 15-20 UT shows how sensitive the winds are to ion drag within the dusk cell.

Figure 10a shows the histogram of the frequency distribution of the ratios of CHAMP/FPI 1-hour averaged cross-track zonal wind magnitudes from Figures 7 and 8. Figure 10b shows the UT dependence. The

Formatted: Superscript

Formatted: Superscript

Formatted: Font color: Auto

Longyearbyen ratios cluster in the range 1.0 - 2.5, while the Kiruna ratios are far more widely spread. Overall there is a general trend for the satellite wind magnitudes to be larger by a factor of 1.5 - 2.0, with median values of 1.7 for Longyearbyen (24 hours coverage) and 1.3 for Kiruna (1530-0530 UT coverage). There does not seem to be any clear pattern when the UT-dependent frequencies of the ratios are plotted in Fig 10b, except for a tendency for the more extreme ratios to occur during the midnight period, when the 630 nm emission is weakest, and the FPI winds have the largest error bars. Even if the midnight measurements are excluded, there is a wide range of values generally greater than 1.0.

Fig 10a, b Frequency distribution of the ratios of CHAMP/FPI one-hour averaged zonal wind magnitudes observed in the winter period for solar max under moderately active conditions (2- ≤ Kp < 4+) for Longyearbyen (blue) and ~~Kiruna~~KEOPS (red). Fig 10a shows the frequency distribution of the CHAMP/FPI ratios, and Fig 10b shows the UT dependence of the ratios.

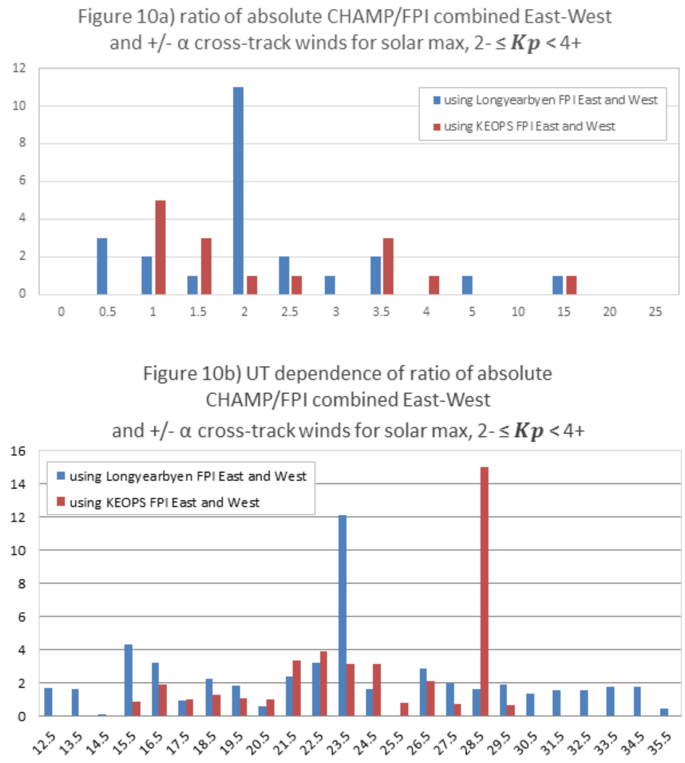

Fig 9 Frequency distribution of the ratios of CHAMP/FPI one-hour averaged zonal winds observed in the winter period Nov-Jan for 2001-2004solar max under moderately active conditions (2- ≤ Kp < 4+) for Svalbard Longyearbyen (redblue) and Kiruna (bluered). Fig 9a) shows UT dependence of ratios, and Fig 9b) shows frequency distribution of ratios.

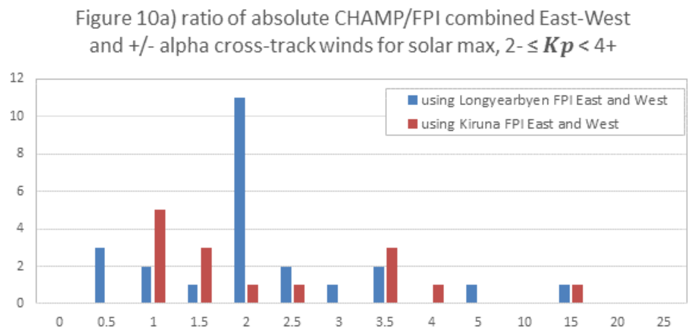

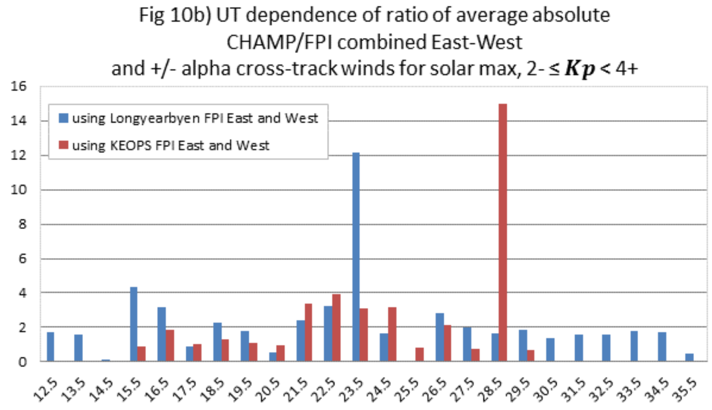

Figure 9a) UT dependence of average CHAMP/KEOPS magnitudes

Figure 9 shows a histograms of a) the UT dependence and b) the frequency distribution of the ratios of CHAMP/FPI average zonal wind magnitudes observed in the winter period Nov-Jan for 2001-2004 for under moderately active conditions (2- ≤ Kp < 4+) for Kiruna and Longyearbyen. The UCL FPI zonal winds observed to the East and West have been averaged into 1 hour bins to match the CHAMP averages of the ascending and descending zonal winds. The Longyearbyen ratios cluster in the range 1.0 - 2.5, while the Kiruna ratios are far more widely spread. Overall there is a general trend for the satellite wind magnitudes to be larger by a factor of 1.5 - 2.0, with median values of 1.8 for Kiruna and 1.4 for Longyearbyen.

Formatted: Font: 9 pt

Formatted: Don't adjust space between Latin and Asian text, Don't adjust space between Asian text and numbers

6. Discussion

We have shown that there is a similar phase, but a considerable difference between the average zonal wind magnitudes measured by the CHAMP satellite and the ground-based FPIs for a polar cap and auroral site during northern winter months. Our premise is that the large molecular viscosity of the upper thermosphere should minimise any vertical structure in the winds above around 250 km altitude. The difference in wind magnitudes could have various explanations. It could be that A) we are mistaken about the vertical structure of winds; or B) that there is a problem with the scaling of the two methods of measurement; or C) the measurement procedures introduce differences, e.g. in-situ versus remote integration; comparison of different spatial and/or temporal resolutions. There may be other, unexpected, reasons for the mainly amplitude differences in the measurements.

With respect to hypothesis A: the CHAMP satellite zonal winds are of a similar magnitude to the original GOCE satellite winds (Liu et al., 2016 and Visser et al., 2019), and to the UCL CMAT2 model simulations. However, while the CHAMP satellite altitude was between 350-400 km, the GOCE satellite had an unusually low altitude around 250 km, which was close to the FPI 630 nm emission peak altitude. The CMAT2 winds are typical of values from other GCMs, which were largely calibrated against measurements by satellites in the 1970s and 1980s, in particular the DE-2 satellites. Killeen et al (1984) found a good agreement between the FPI at Longyearbyen (then called the University of Ulster FPI, and subsequently the University of Alaska FPI) for observations in December 1981. Though later Hedin et al. (1991) found that on average the satellite wind measurements were larger. ~~This is because the~~The DE-2 satellite measurements were made using the Wind and Temperature Spectrometer (WATS), rather than derived from satellite drag measurements. The DE-2 satellite flew from August 1981 to February 1983, which means that the average monthly F10.7 flux included some of the highest solar flux values of the last 30 years. This may account for why ~~the~~ physical and empirical GCMs calibrated from that period have such large wind values. The two decades since 2000 have recorded the most sustained and low F10.7 flux levels since the satellite era began.~~.~~

With respect to hypothesis B: the satellite drag community are already aware of a scaling issue. Defining the drag coefficient is the largest source of error. Bruinsma et al (2014) had to multiply GOCE densities by a factor of 1.29 to match the real-time High Accuracy Satellite Drag Model (Storz et al., 2005). HASDM uses data assimilation from the orbits of 75-85 inactive payloads and debris over 200-900 km altitude that are tracked by the Space Surveillance Network (SSN) and is considered a benchmark by that community. Recently March et al. (2019), reanalysed thermospheric densities derived from very precise satellite accelerometers and GPS acceleration using high fidelity satellite geometries. The densities for all the spacecraft surveyed were greater than those derived using surfaces defined by flat panels; and more consistent with each other. The CHAMP and

Formatted: Don't adjust space between Latin and Asian text, Don't adjust space between Asian text and numbers

GOCE densities were found to be 11% and 9% larger. Although there is no simple link between densities and winds, this re-scaling of densities gives an indication that it may be necessary to scale winds down for the same measured acceleration (see section 6.3 and Eq. 6).

With respect to hypothesis C – the assumptions of the FPI and CHAMP measurement techniques are discussed in the following sections 6.1-6.3.

Formatted: Font: (Default) Times New Roman

Formatted: Font: (Default) Times New Roman

6.1 Considering the molecular viscosity of the upper thermosphere

Let us first consider hypothesis A, that the CHAMP and ground-based FPI average zonal measurements are both correct, and that the factor of 1.5-2.0 difference in wind magnitudes is due to the 100-150 km difference in the altitude of the measurements. Conventional fluid dynamics theory predicts that the molecular viscosity is very high in the upper thermosphere owing to the very low particle densities at these altitudes. The viscosity of a fluid determines how resistant it is to shear forces that cause adjacent layers to move at different speeds. Turbulent viscosity dominates the atmosphere below about 100 km, but molecular viscosity dominates the upper atmosphere. The molecular viscosity of the upper thermosphere is very large, and in the CMAT2 model the molecular viscosity η, is given by Eq. (~~5~~2) (Harris, 2001; Hood, 2018) which is based on Dalgarno and Smith (1962)~~, and Banks and Kockarts (1973).~~

$$\eta = 4.5e^{-5} \times \left(\frac{T}{1000}\right)^{0.71} \qquad (\sout{5}2)$$

As a consequence of large viscosity, there is little shear between the different altitude layers above ~200 km for both winds and neutral temperatures (hence the name thermosphere representing an iso-thermal behaviour). The issue raised in this paper is that the difference between CHAMP and FPI wind magnitudes is too large to be consistent with the assumption of large viscosity over this range of altitudes.

Fig 11~~0~~ CMAT2 zonally averaged zonal winds for 00UT at December solstice 2008 (solar minimum conditions) to demonstrate the effect of drastically reducing the molecular viscosity in order to raise the altitude where winds become independent of altitude. The left panel shows isobars for a standard simulation, while the right panel represents a simulation where the molecular viscosity is 100 times smaller (from Hood, 2018).~~.~~

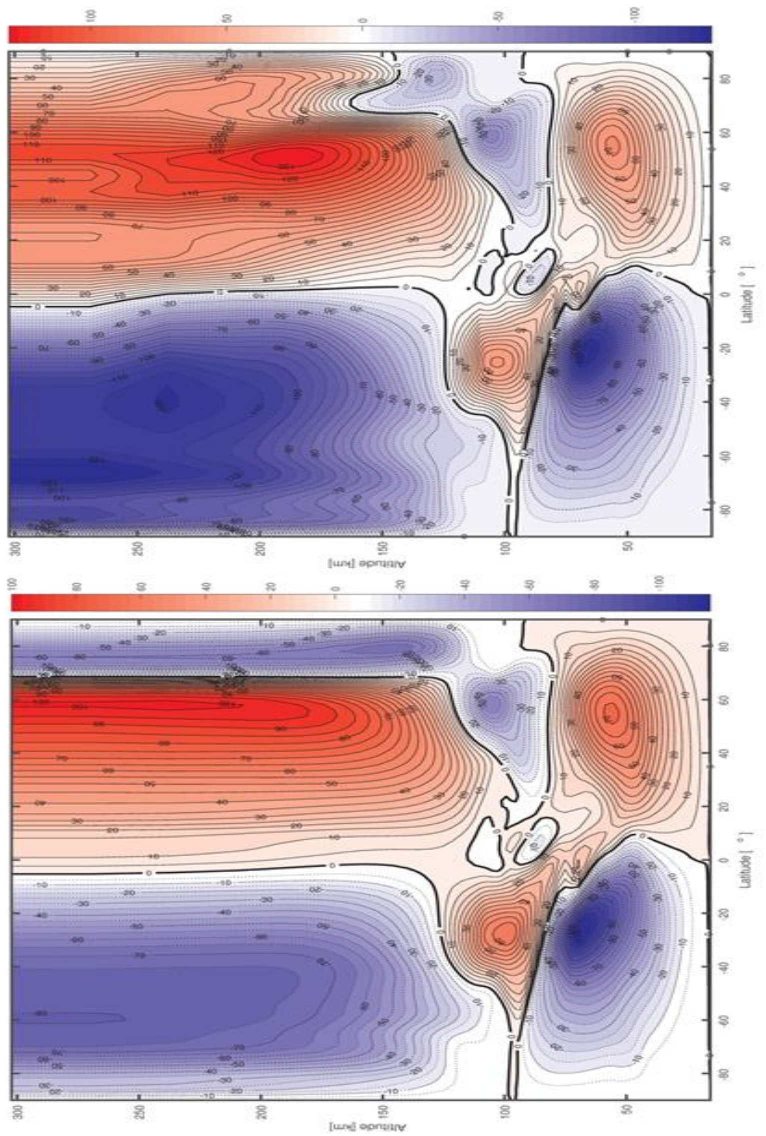

Figure 11~~0~~ shows two versions of the CMAT2 zonally averaged zonal winds for 00 UT for December solstice 2008 (solar minimum conditions) from Hood (2019). These are latitude-height plots, where the height is from 15 km to 300 km. From about 250 km the contour lines become near vertical because the large molecular viscosity of the upper thermosphere minimises the shear in the winds. The left hand plot is the standard run using standard values of molecular viscosity. The right hand plot shows the contours for a simulation where the molecular viscosity has been reduced by a factor of 100. The variation of the molecular viscosity with respect to temperature (and consequently height for our purposes) has been tested theoretically and experimentally by Dalgarno and Smith (1962), and the factor of 100 is an unrealistic extreme used to test the model. The consequence is that the height at which contours become vertical is raised to closer to 280 km. This is a small difference and certainly does not account for the apparent vertical gradient indicated by the difference between the CHAMP and FPI zonal winds.

Song et al. (2009) state ~~studied the local response of the ionosphere and thermosphere to changes of the magnetospheric convection at polar latitudes on the basis of a 1-D three-fluid model approach. It includes ions, electrons, and neutral particles and their collisions within the polar cap, hence describing the coupled processes between the magnetosphere, ionosphere, and thermosphere in the vertical direction along the magnetic flux tubes. In this self-consistent 1-D solution, the neutral wind speed is obtained as a function of height. The model describes the dynamic response of the ionosphere/thermosphere after relatively rapid changes of the magnetospheric convection within about 10-20 Alfvèn wave travel times (or 15-30 minutes) within the magnetosphere between conjugated hemispheres, or between the ionosphere and the magnetopause, until the system reaches its steady state again. It is shown~~ that the fastest acceleration of the neutrals occurs near 350 km in the F layer, where the effective neutral-ion collision frequency maximizes (see their Figs. 6 and 7~~ of Song et al., 2009~~). Considering the dynamic character of frequent changes of the IMF and the magnetospheric convection, the stronger accelerations at F2 layer heights could result in temporary vertical neutral wind gradients. However, the 1-D model approach neglects forces due to neutral pressure and effective molecular viscosity in the 3-D continuum of the upper thermosphere~~ (Song et al., 2009)~~. To describe correctly the long-range coupling on time scales from longer than few seconds to less than 30 min, the inductive effect (Faraday's law) as well as the dynamic effect of the neutrals, in particular (acceleration terms), need to be considered (Song and Vasyliunas, 2013). This poses a challenge for future modelling efforts of the M-I-T system.

Recently Vadas and Crowley (2017) published results from observations of 10 Travelling Ionospheric Disturbances at ~283 km altitude, observed in 2007 with the TIDDBIT ionospheric sounder near Wallops Island, USA. They used ray tracing on the TIDs and simultaneously measured a peak in the neutral wind at ~325 km altitude using a sounding rocket. They found a serious discrepancy between where the gravity waves were predicted to dump energy using conventional dissipative theory, and the observations from TIDDBIT and the rocket. Conventional theory predicted that all the gravity waves should have dispersed at a scale height below the rocket measurement. Consequently they have challenged convention and proposed that the molecular viscosity should not increase as rapidly with altitude above 220 km. This may account for some of the difference between the CHAMP and FPI zonal winds, ~~and~~ but will need to be tested in future modelling studies.

6.2 FPI Doppler shift to wind speed procedure

Hypothesis B is that the FPI and/or CHAMP observations may need to be re-scaled. To start with the FPIs we will look at the calculation of the Doppler shift and then at the height integration procedure of a ground-based FPI.

The calculation of the wind speed requires few assumptions, though the process of fitting the FPI fringes is more complicated (e.g. Makela et al., 2011). The wind speed *u* is determined from the Doppler shift of the wavelength $\Delta\lambda$ of the moving volume of gas which emits at wavelength λ, where the free-space wavelength is λ_o and the speed of light *c* (Eq. ~~7~~3).

$$\lambda = \lambda_o\left(1+\frac{u}{c}\right) = \lambda_o + \Delta\lambda \qquad (~~7~~3)$$

The speed of the volume of gas *u* is given by Eq. (4~~8~~), which is proportional to the ratio of the Doppler shift in fringe peak position (in bins) Δx; and the free spectral range (FSR), Δx_{FSR}. The FSR is the equivalent wavelength shift to ~~shift~~ re-position a fringe from overlapping one order of the baseline wavelength λ_o, to the next order. The other terms in Eq. (~~8~~4) are the refractive index μ of the medium between the etalon plates and the separation of the plates, *d* (Hecht and Zajak, 1980).

$$u = \left(\frac{\Delta x}{\Delta x_{FSR}}\right)\left(\frac{c\lambda_o}{2\mu d}\right) \qquad (~~8~~4)$$

The etalon gap is evacuated so μ=1, and the other parameters are known. Thus for example, for an etalon gap *d* = 10 mm, emission λ_o = 630 nm, free spectral range Δx_{FSR} = 150 bins, a Doppler shift of 1 bin (Δx = 1 bin) would represent a wind of 63 ms^{-1}.

All the parameters for the scaling of the FPI winds in this equation are known. There is the issue of determining the zero Doppler shift baseline because there is no laboratory source of the excited atomic oxygen. However, the method used to determine the baseline (i.e., using a helium-neon source with the assumption that the vertical component of the wind is negligible) introduces an average systematic offset error of at most 10-20 ms^{-1}, which is small compared with horizontal wind magnitudes (Aruliah and Rees, 1995).

Fig 12~~1~~ left: height profile of CMAT2 zonal winds at Svalbard. Right: height profile of the red line emission intensity profile from the Vlasov et al (2005) model.

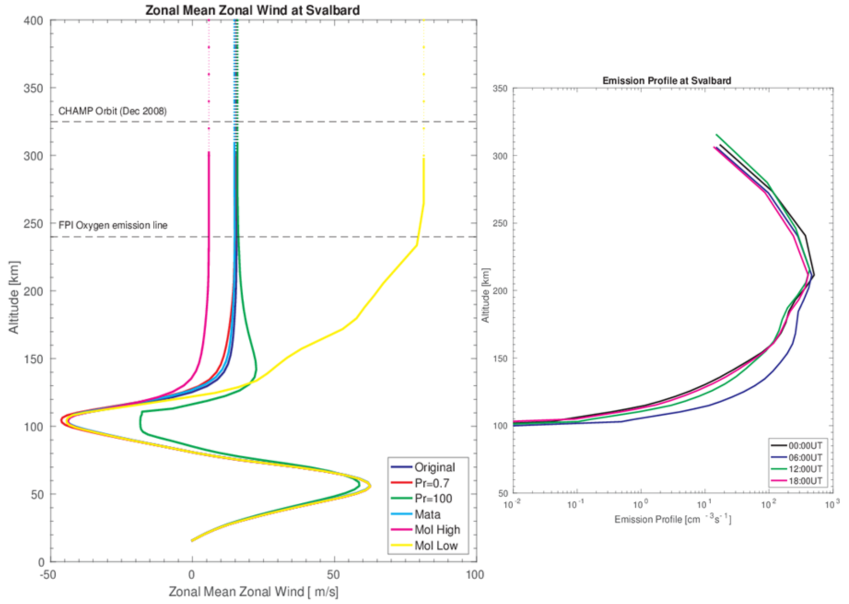

Figure 12 illustrates how ground-based FPIs make measurements of the neutral winds at 240 km altitude. The left plot shows a height profile of the CMAT2 zonal mean zonal winds at the latitude of Longyearbyen. There are 6 simulations to demonstrate the effect on the height profile of the zonal mean zonal winds when changing the viscosity. CMAT2 uses a viscosity term that is the weighted mean divided by the scale height of two coefficients of viscosity: the molecular viscosity μ_m; and the turbulent viscosity μ_t. The simulations represent a comparison with the original molecular viscosity (dark blue). The other lines are for low (yellow - divided by 100) and high molecular viscosities (pink - doubled). The low and high turbulent viscosities are represented by the Prandtl numbers 0.7 (red) and 100 (green), where 2 is the default value used in CMAT2. The Prandtl number is related to the height at which gravity waves deposit momentum (Liu et al., 2013) and so may have relevance for the Vadas and Crowley experiment (2017). The light blue line labelled "Mata" is an intermediate profile. As can be seen, the molecular viscosity dominates in the thermosphere above 100 km and at the altitudes where the FPI is measuring. The dark blue and yellow lines are ~~effectively~~representative of a vertical slice of Figure 11 left and right, respectively, for the latitude of Longyearbyen.

The right hand plot of Figure 12 is a CMAT2 height profile of the 630 nm (red) line emission intensity based on the Vlasov et al. (2005) model at 00UT, 06UT, 12UT and 18UT. The red line emission at night is dominated by dissociative recombination of molecular oxygen (O$_2^+$ + e -> O* + O)~~ (e.g. Vlasov et al., 2005)~~. The altitude distribution of the 630 nm emission has a peak emission altitude of between 220-250 km, ~~(e.g. Link and~~

Formatted: Font color: Auto

Cogger, 1988; Vlasov et al., 2005). However, the emission profile also has a full width at half maximum intensity of around 50-70 km, i.e. sampling altitudes tens of km below and above the emission peak. The ground-based FPI observes a height-integration of the emission along the line-of-sight. The measured Doppler shift is therefore an integration of the Doppler shifts at all altitudes, weighted by the emission profile. However, there are several reasons to justify why we are confident that the FPI provides a good sample of the winds at ~240 km altitude. The excited atomic oxygen state in the O (^{1}D-^{3}P) transition is a forbidden transition with a long life-time of ~110 sec (Bauer, 1973), which allows the excited atoms to thermalise before emission and be representative of the surrounding gas. Below 200 km the molecular composition increases significantly, and the long lifetime means that the 630 nm emission is quenched due to molecular collisions with N_2 and O_2. Consequently we can assume there is minimal contribution of Doppler shifts from below 200 km altitude, which is a region where the neutral wind magnitude has a large height dependence (note that the emission intensity x-axis is a log scale; and that, the horizontal winds at 100 km altitude are a few tens of ms^{-1} while at 250 km altitude are a few hundreds of ms^{-1}). Above the altitude of the emission peak the flux falls off rapidly with altitude, and also with distance from the FPI, which minimises the contribution of winds from the region above. In addition, above 250 km the wind magnitudes begin to reach an asymptote. It therefore would be expected that the satellites and ground-based FPIs should see very similar speeds and phases. Overall it is suggested thatWith respect to the FPI measured winds, the contribution of winds below the peak emission height may result in a small underestimate of the winds at ~240 km altitude by no more than about 10% due to the contribution of winds below the peak emission height, which , is investigated later in this section by modelling.

Figure 11 illustrates how ground-based FPIs make measurements of the neutral winds at 240 km altitude. The left plot shows a height profile of the CMAT2 zonal winds at Longyearbyen. On the right is a height profile of the 630 nm (red) line emission intensity based on the Vlasov et al. (2005) model. The red line emission at night is dominated by dissociative recombination of molecular oxygen (O_2^+ + e -> O* + O) (e.g. Vlasov et al., 2005). The ground-based FPI measures the Doppler shift of the gas, height integrated through a volume along the line-of-sight. This means that all winds at all altitudes contribute to the measurement, but are weighted by the red line emission intensity. The emission height profile shows a sharp velocity gradient below 200 km, but owing to quenching of the emission through collisions, there is little emission below 200 km (note the emission intensity x-axis is a log scale), and therefore a minimal contribution to the height-integrated line-of-sight wind measurement. Above 200 km the wind magnitudes begin to reach an asymptote. It therefore would be expected that the satellites and ground-based FPIs should see very similar speeds and phases. The tristatic FPI experiments by Aruliah et al (2005) and bistatic experiments by Anderson et al (2012) indicated that the winds, neutral temperatures and 630 nm intensities were closely matched if the geometry assumed an emission altitude of around 240 km. However, during auroral activity, when there is E-region precipitation, the red line emission altitude can be lower, perhaps as low as 200 km. This means that the FPI samples lower altitudes. Recently Gillies et al. (2017) used all-sky imagers to triangulate the peak emission height of the 630 nm emission. They found that discrete auroral arcs showed a characteristic height of 200km. The effect of particle precipitation in lowering the emission height was earlier noted by Sica et al. (1986). They illustrated how decreased thermospheric temperatures measured by a Fabry-Perot spectrometer at College, Alaska, were consistent with

Formatted: Font color: Auto

Formatted: Font color: Auto

Formatted: Font color: Auto

lower MSIS temperatures (Hedin et al., 1977) when weighted by a modelled emission height profile. However, aurorae are limited to high latitudes and occur infrequently as illustrated by Figure 132, which shows the frequency distributions of Kp values for the years (top) 2001-2003 representing solar maximum; and (bottom) 2000-2009, i.e., for most of the period of the CHAMP lifetime. Aurora generally occur during active periods when Kp > 4-5. Thus emission heights of 200 km are the exception rather than the rule, and affect the average only minimally.

Fig 132 Frequency distribution of Kp values. Top: 2001-2003 representing solar maximum. Bottom: 2000-2009 covering most of the period of the CHAMP lifetime.

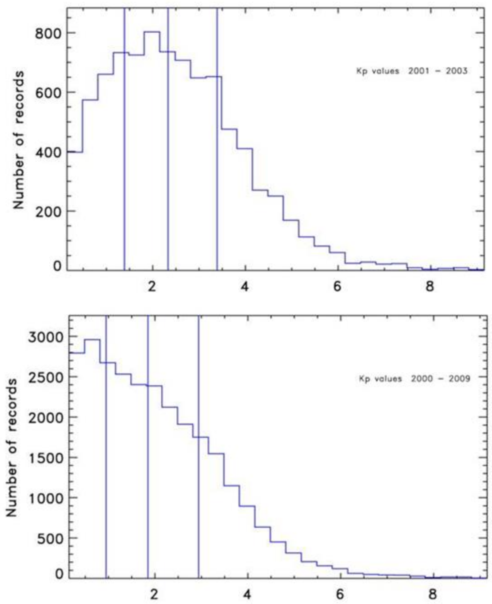

Fig 14~~3~~ top: CMAT2 zonally averaged zonal winds for a quiet day on 1st December 2007 at Longyearbyen (left) and Kiruna (right) for the winds at 180, 200 and 240km for comparison with the height integrated winds weighted using an emission intensity profile from the Vlasov et al (2005) model. Bottom: the same for active conditions on 20th March 2015.

Formatted: Adjust space between Latin and Asian text, Adjust space between Asian text and numbers

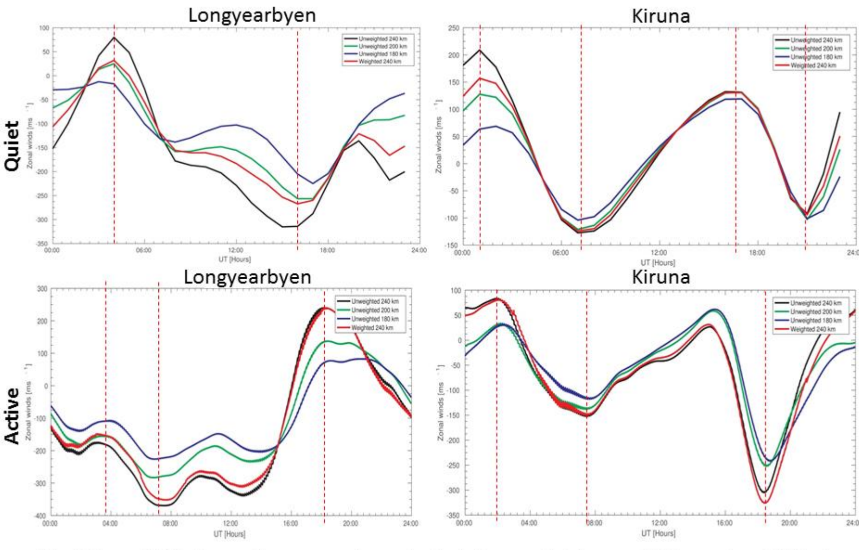

In order to assess by how much the FPI height integration method is underestimating winds, CMAT2 winds at 240 km are compared to a column integration average of CMAT2 winds weighted by the emission intensity profile. Here the Vlasov et al (2005) model is applied with constants provided by Yiu (2014), and with CMAT2 winds interpolated to 10 km intervals for the integration. Figure ~~13~~ 14 compares the CMAT2 zonally averaged zonal winds at three heights: 180 (blue), 200 (green) and 240 km (black) with height integrated winds (red) for a quiet day run on the 1st December 2007 (top panels) and an active day run on the 20th March 2015 (bottom panels) for both Longyearbyen (left column) and Kiruna (right column). Figure 15~~4~~ outlines the CMAT2 model global view of the unweighted and weighted winds at 240km for 00, 06, 12 and 18UT.

Fig ~~14~~15: CMAT2 global zonal winds for a quiet day on 1st December 2007 for the winds at 240km and the height integrated winds weighted using an emission profile from Vlasov et al (2005) model. From top left: 0UT, 6UT. From bottom left: 12UT, 18UT.

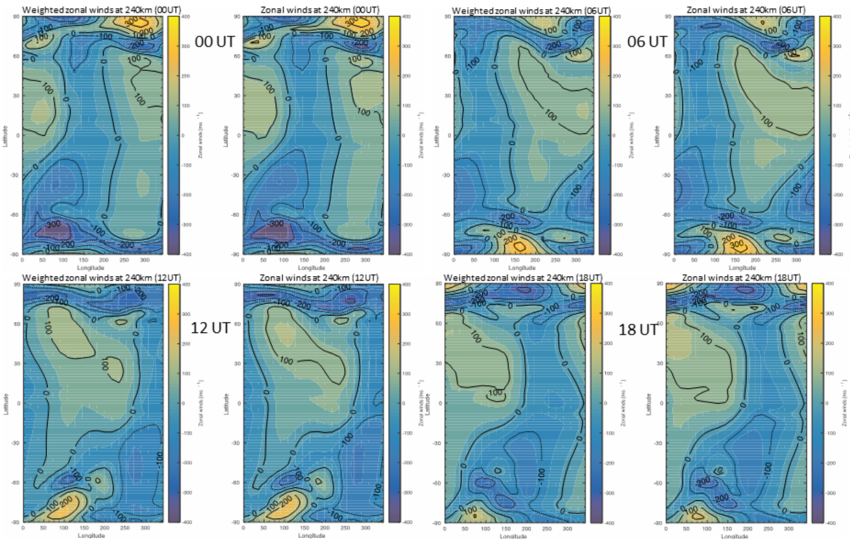

Figure ~~13~~ 14 indicates that there are some significant differences between zonally averaged zonal winds with or without height integration. The lower the altitude, the smaller the wind magnitude. There is also a slight change in phase (to aid the eye these are indicated by vertical dashed lines placed at turning points for the weighted winds). This is due to the increased collision frequency at lower altitudes due to greater density, and the consequent shift in balance between pressure gradient and ion drag. When we look at the averaged diurnal variation of the CHAMP and FPI winds, their phases are almost exactly the same. This would not be the case if the FPI was observing winds dominated by Doppler shifts at 190 km altitude, where the phase would be significantly different because the pressure gradient increases its dominance at lower altitudes. Comparing the CMAT2 December 2007 model zonally averaged zonal winds at 240 km with the height integrated winds, the most significant difference is for Longyearbyen during quiet conditions, which on calculating overall mean values produces a 19% difference, that during active conditions reduces to a difference of 12%. The reverse seems the case for Kiruna as the mean percentage difference increases from 3% to 14% between the quiet and active days respectively. Note that the wind speed scales are different for each panel. For each time-series there is no simple systematic trend. Figure ~~14~~ 15 demonstrates these dissimilarities on a global scale; here the zonal winds appear to be slightly more westward, as the e~~E~~astward winds are diminished and the w~~W~~estward winds enhanced. However, this is not the case for all times of day shown here, and ~~is~~ does not visibly affect~~ing~~ the wind distributions to any large extent.

6.3 CHAMP cross track wind procedure

Satellites have provided global coverage of accelerometer measurements since 2001, in particular, the CHAMP satellite (e.g. Schlegel et al., 2005) and GRACE satellites (e.g. Tapley et al., 2004). These measurements of satellite drag have been converted to measurements of thermospheric mass density (e.g. Liu et al., 2005) and cross-track thermospheric wind measurements (e.g. Sutton et al, 2007, Liu et al., 2006, Förster et al., 2008). Thermospheric mass density was primarily estimated using Eq. 5 where ~~using Eq. 6, where~~ a is the satellite acceleration, ρ the neutral mass density of the air, C_d refers to a dimensionless drag coefficient, using a constant frontal area A_{ref} of the satellite with mass m, and total velocity V relative to the atmosphere in the ram direction given by the unit vector $\hat{v}$. This equation has been used for a first simple cross-track wind estimation, where the area and wind component were replaced by the horizontal side view and neutral wind direction perpendicular to the bulk flow, respectively.

$$a = -\frac{1}{2}\rho\frac{C_d}{m}A_{ref}V^2\hat{v} \qquad (~~6~~5)$$

For the first analysis, Liu et al. (2005) explained that they used a fixed drag coefficient value of $C_d = 2.2$. This is a de-facto standard value used for compact satellite orbit computations since the 1960s (e.g. Cook, 1965). This value was adopted by Jacchia when constructing his thermosphere density model, based on physical drag modelling of spherical satellites (Jacchia and Slowey, 1972). The drag coefficient is acknowledged to be very difficult to quantify, as is discussed extensively by, for example, Moe et al. (1995). The importance of the value of C_d is acknowledged by Liu et al (2006) and others who use the data, since it affects the scaling of the density and wind calculations. However, their interest was in the relative density and wind structures, rather than absolute values.

Since then the analysis has been refined considerably by taking into account lift, sideways, as well as drag forces on the satellite, resulting in smaller wind magnitudes as described by Doornbos et al. (2010). The GOCE satellite winds are closer in magnitude to ground-based FPI measurements (Dhadly et al., 2017), though still systematically larger in magnitude, where the difference has been found to increase with latitude. The systematic residual line-of-sight GOCE wind varied between 20 ms^{-1} at 50° MLAT to a maximum 150 ms^{-1} at 85° MLAT (see Figure 2 from Dhadly et al., 2018).

Another consideration is that CHAMP measures the cross-track wind component (Figures 1~~-an~~-2 and 3-4~~d 2~~) which deviates from the pure zonal direction as measured by the FPIs (Figures ~~3~~ 6 and ~~4~~7). The geometry can be critical, in particular for the high-latitude Longyearbyen FPI, because the cross-track deviates from the zonal direction by about 13.3~~5~~° in each direction respectively for the ascending and descending orbits. The meridional wind component at these high latitudes is much larger than the zonal one, so that the larger CHAMP measurements at this FPI could also (at least partially) be due to an "admixture" of the meridional wind component and the zonal wind. This has been discussed in section 5.1 to account for the difference between the average zonal winds measured during the ascending and descending orbits. To deal with this the UCL FPI zonal winds observed to the East and West are projected onto the CHAMP ascending and descending cross-track directions, and then averaged into 1-hour bins, thus replicating the CHAMP zonal wind averages (see Figures 7

Formatted: Font: 12 pt
Formatted: Font: 12 pt
Formatted: Font: 12 pt
Formatted: Font: 12 pt
Formatted: Font: 12 pt
Formatted: Font: 12 pt
Formatted: Font: 12 pt
Formatted: Font: 12 pt
Formatted: Font: 12 pt
Formatted: Font: 12 pt
Formatted: Font: 12 pt
Formatted: Font: 12 pt
Formatted: Font: 12 pt

and 8). Despite this re-calculation there is a wide range of values of the CHAMP/FPI ratios (see Figure 10a, b), which reinforces the message that the satellite aerodynamic coefficients are difficult to determine absolutely, ~~on top~~which is in addition to some ~~of a~~ systematic factor between the CHAMP and FPI measurements.

6.4 Comparison with EISCAT radar ion velocities

Finally, a very important consideration is how the average winds compare with ion velocities. At high latitudes the ion velocities are generally larger than the neutral winds owing to the *E* x *B* drift driven by the magnetospheric electric field. Davies et al (1995) provided a statistical analysis of E- and F- region ion velocities observed on 20 March 1996 in order to compare measurements by the EISCAT incoherent scatter radars and the CUTLASS coherent scatter radar. The scatter plot of ion velocities from this study (their Figure 5) indicated a cluster of values in the range of a few hundred ms^{-1}, with only a small fraction of measurements greater than 500 ms^{-1}.

Fiori et al (2016) compared ion velocities measured by the Electric Field Instrument on Swarm with the CS10 statistical ionospheric convection model by Cousins and Shepherd (2010) which is based on 8 years of data (1998-2005) collected by 16 SuperDARN coherent scatter radars. The climatology represented by the CS10 model in Fiori et al's Figure 3a indicates speeds in the few hundreds of ms^{-1}, while the instantaneous values along the Swarm satellite pass ~~in~~ (their Figure 3d) show much stronger drift peak values on the resolution level of seconds or shorter. Even after allowing for offsets, their 1-sec resolution corrected cross-track ion drifts achieve horizontal velocities well over ~~a~~ 1,000 ms^{-1}, which probably indicates the highly dynamic behaviour in the auroral regions compared with quasi-stable conditions used for empirical models. However, recently Koustov et al. (2019) compared the Swarm cross-track ion drifts with the SuperDARN radar network and found that the Swarm ion velocities are a factor of 1.5 larger. They suggest reasons for the disparity, including refining the calibration of Swarm and the differences in spatial/temporal resolution.

Aruliah et al. (1996) presented the seasonal and solar cycle variation of hourly averaged ion velocities from 300 days of EISCAT Tromsø UHF radar measurements between 1984-1990. The tristatic EISCAT radar observations for an altitude of 275 km were collected from Common Programmes 1, 2 and 3, at time resolutions of 2-3 mins, with full 24 hours coverage. The hourly averaged ion velocities for December solstice periods were up to 100-200 ms^{-1}, and the largest average ion velocities were around 300 ms^{-1} during the March equinox period at solar maximum. Aruliah et al. (2005) later reported observations of a common volume using a configuration of tristatic FPI observations of the thermospheric winds and temperatures co-located with tristatic EISCAT radar measurements of ionospheric parameters at 250 km altitude. The observations showed that the neutral winds were on average around 50% of the magnitude of the ~~15 min average~~ ion velocities when averaged over 15 min.

Formatted: Font color: Auto

Formatted: Font: Italic

Formatted: No underline

Formatted: Font: Italic

Griffin et al. (2004) determined seasonal and solar cycle climatologies of meridional winds at Kiruna using FPI Doppler shifts, and derived from field-aligned ion velocities (Salah and Holt, 1974), which were compared with physical (CTIM, Fuller-Rowell et al., 1988) and empirical models (HWM, Hedin et al, 1988; MWM, Miller et al., 1997). The climatologies all showed meridional winds up to ~250 ms^{-1}. Although this method does not give the zonal wind magnitude, it gives some indication of typical magnitudes owing to the diurnal variation of winds seen by a single site as the Earth rotates.

Förster et al. (2008) presented a statistical comparison of observed averaged neutral wind velocities within the polar cap (magnetic latitudes > 80°) for the year 2003 showing the dependence on the IMF orientation based on statistical analyses of CHAMP accelerometer data with average ion drift estimates for the same time interval and IMF conditions based on EDI Cluster measurements. These comparisons were done for both the Northern and the Southern Hemisphere separately in their Tables 1 and 2, respectively. Depending on the IMF clock angle orientation, the ratio between average neutral wind magnitudes and average ion drift speeds varies between about 60% and around 100%. Interestingly, there is a characteristic interhemispheric difference with respect to the IMF orientation and slightly larger ion drift velocities on average in the Northern Hemisphere (cf. Förster and Cnossen, 2013; Förster et al., 2017), but the overall average amounts to a ratio of about 0.90 to 0.95 for, note well, within the polar cap region > 80° magnetic only. The FPI in Longyearbyen at 75.4° N (see Table 2) comes closest to this region. Ion drag is the dominating forcing term here for the neutral gas, while near the auroral ~~ring~~oval, where the KEOPS FPI station in Kiruna at 65.1° N is located, the balance between the different forces, in particular pressure gradient terms, Coriolis and centrifugal forces, and ion drag, play a role. There the ratio between the average neutral wind and ion drag magnitudes is certainly smaller, corresponding to the EISCAT observations cited above.

7 Conclusions

A comparison is presented here of thermospheric zonal winds during winter months between 2001-2007 measured by the CHAMP satellite in the altitude region 350-400 km, and by ground-based FPIs, at Kiruna and Longyearbyen, measured at about 240 km altitude. The satellite accelerometer measurements of drag are used to derive cross-track winds, while the FPIs use the Doppler shift of the 630 nm emission. The satellite measurements are collected for a region within 2° latitude of the FPI sites, which is within the field of view of the FPI East and West look directions. The phases of the winds agree very well, but the CHAMP average zonal winds are a factor 1.5-2.0 larger than the FPI average zonal winds. The factor is not simple. In particular there is a difference in the factor for the auroral site and the polar cap site, so it appears that the factor is dependent on location, possibly latitude. The factor also appears to have an irregular time dependence.

The UCL Longyearbyen FPI winds are consistent with FPI measurements made 20 years previously by the University of Alaska using a different FPI and detector (photometer in 1980, EMCCD in 2001). Earlier studies of average ion velocities from the EISCAT Tromsø UHF radar compared with the UCL FPI at KEOPS indicate that in the auroral zone the average ion velocities are about twice the average neutral wind speeds (Aruliah et al., 1996 and 2005). However, the CHAMP average ~~KEOPS~~ zonal winds at KEOPS presented here have magnitudes similar to the average ***ion*** velocities of the December solstice values presented by Aruliah et al

(1996). This is probably the key argument indicating that the CHAMP magnitudes are too large. It is important to determine the absolute wind values correctly since the difference between the ion and neutral winds determine the amount of Joule heating of the thermosphere.

Satellites play a crucial role in upper atmosphere research by filling in the extensive gaps between ground-based observations. Satellites provide 3-dimensional coverage at high spatial resolution, in addition to high temporal resolution. Meanwhile, ground-based instruments are sparse, land-based, and not always operational on a 24/7 basis owing to operational costs (e.g. incoherent scatter radars) or observing constraints (e.g. only night-time and clear sky observations for optical instruments). Having uncovered this discrepancy between ground-based FPI optical measurements and satellite drag measurements of winter winds, it is imperative to determine if it is a real altitude dependence, or if some re-scaling of winds, is necessary for winds determined from either, or both, of FPI height-integrated Doppler shifts or satellite drag measurements. Both possibilities will affect our current modelling of the upper atmosphere.~~;~~ ~~or whether~~ W~~w~~e may also need to rethink the procedure of comparing different spatial and temporal ~~and temporal~~ resolutions of in-situ satellite versus remote ground-based FPI measurements ~~and~~ in terms of the geometry of cross-track winds at high latitudes.

Author contributions. This paper is the result of many years of collaboration between AA and MF after noticing the significant difference between FPI and CHAMP winds. AA provided the FPI data, MF provided the CHAMP data. RH provided the model simulations, IM provided technical support for the FPIs, and ED provided expertise on converting accelerometer data to winds.

Competing interests. The authors declare that they have no conflict of interest.

Data availability. The CHAMP accelerometer neutral wind observations used in this study are available at http://doi.org/10.5880/GFZ.1.1.2019.001 (Förster and Doornbos, 2019).

*Acknowledgements***.** We thank the staff at the Kjell Henriksen Observatory and ESRANGE for hosting the FPIs and their generous on-site assistance. Support for the FPI operations have come from the European Office of Aerospace Research and Development (grant FA9550-17-1-0019). There has been NERC support of ALA (grants NE/P001556/1 and NE/N004051/1). The CHAMP mission is sponsored by the Space Agency of the German Aerospace Center (DLR) through funds of the Federal Ministry of Economics and Technology, following a decision of the German Federal Parliament (grant code 50EE0944). The data retrieval and operation of the CHAMP satellite by the German Space Operations Center (GSOC) of DLR is acknowledged. EISCAT is an international association supported by research organisations in China (CRIRP), Finland (SA), France (CNRS, till end 2006), Germany (DFG), Japan (NIPR and STEL), Norway (NFR), Sweden (VR), and the

Formatted: Font: Italic

Formatted: Font: (Default) Times New Roman, Italic

Formatted: Font: (Default) Times New Roman

Formatted: Font: (Default) Times New Roman

Formatted: Normal, Don't adjust space between Latin and Asian text, Don't adjust space between Asian text and numbers

Formatted: Font: (Default) Times New Roman

United Kingdom (STFC). We also acknowledge support from the International Space Science Institute for sponsoring meetings of the international team #308 on 'M-I-T Coupling: Differences and similarities between the two hemispheres', which helped this collaboration (http://www.issibern.ch/teams/twohemispheres/).

Formatted: Don't adjust space between Latin and Asian text, Don't adjust space between Asian text and numbers

References:

Anderson, C., Conde, M., and McHarg, M. G.: Neutral thermospheric dynamics observed with two scanning Doppler imagers: 1. Monostatic and bistatic winds, J. Geophys. Res.,117, A03304, doi:10.1029/2011JA017041, 2012.

Aruliah A.L., Rees, D.: The Trouble with Thermospheric Vertical Winds: Geomagnetic, Seasonal and Solar Cycle Dependence at High Latitudes, J. Atmos. Terr. Phys., 57, 597-609, 1995

Aruliah A.L., Farmer, A. D., Rees, D., Brändström, U.: The Seasonal Behaviour of High-Latitude Thermospheric Winds and Ion Velocities Observed Over One Solar Cycle, J. Geophys. Res., 101, 15701-15711, 1996

Aruliah, A. L. and Griffin, E. M.: Evidence of meso-scale structure in the high-latitude thermosphere, Ann. Geophys., 37–46, 2001.

Aruliah, A. L., Griffin, E. M., Aylward, A. D., Ford, E. A. K., Kosch, M. J., Davis, C. J., Howells, V. S. C., Pryce, E., Middleton, H., Jussila, J.: First direct evidence of meso-scale variability on ion-neutral dynamics using co-located tristatic FPIs and EISCAT radar in Northern Scandinavia, EISCAT workshop special issue Annales Geophys., 23, 147-162, 2005

Bauer, S.J.: Physics and chemistry in space, Vol 6 of Physics of planetary ionospheres, Springer-Verlag, 1973

~~Banks, P.M. and Kockarts, G.: Aeronomy: Parts A and B. Academic Press: New York, 1973~~

Bruinsma, S. L., Doornbos, E., Bowman, B.R.: Validation of GOCE densities and evaluation of thermosphere models Advances in Space Research, Volume 54, Issue 4, 576-585.10.1016/j.asr.2014.04.008, 2014.

Cook, G.E.: Satellite drag coefficients, Planet. Space Sci., 13, 929, 1965

Cousins, E. D. P., and S. G. Shepherd (2010), A dynamical model of high‐latitude convection derived from SuperDARN plasma drift measurements, J. Geophys. Res., 115, A12329, doi:10.1029/2010JA016017.

Dalgarno, A., and Smith, F. J.: The thermal conductivity and viscosity of atomic oxygen, Planet.Space.Sci., 9, 1-2, 1962.

Davies, J.A., Lester, M., –Milan, S.E., Yeoman, T. K.: A comparison of velocity measurements from the CUTLASS Finland radar and the EISCAT UHF system, Ann.Geophys., 17, 892-902, 1999.

Deehr, C. S., Sivjee, G. G., Egeland, A., Henriksen, K., Sandholt, P. E., Smith, R., Sweeney, P., Duncan, C., Gilmer, J.: Ground-based observations of F region aurora associated with the magnetospheric cusp, J. GEOPHYS. RES., 85, 2185-2192, 10.1029/JA085iA05p02185, 1980.

Dhadly, M., Emmert, J., Drob, D., Conde, M., Doornbos, E., Shepherd, G., Makela, J., Wu, Q., Niciejewski, R., and Ridley, A.: Seasonal dependence of northern high-latitude upper thermospheric winds: A quiet time

Formatted: Font: Times New Roman, 10 pt

Formatted: Font: 10 pt

Formatted: Font: Times New Roman, 10 pt

climatological study based on ground-based and space-based measurements, Journal of Geophysical Research (Space Physics), 122, 2619-2644, 10.1002/2016JA023688, 2017

Dhadly, M., Emmert, J., Drob, D., Conde, M., Shepherd, G., Makela, J., Wu, Q., Niciejewski, R., and Ridley, A.: Seasonal Dependence of geomagnetic active-time northern high-latitude upper thermospheric winds, J. GEOPHYS. RES., 123, 739-754, https://doi.org/10.1002/2017JA024715, 2018

Doornbos, E, Ijssel, J., Lühr, H., Förster, M., and Koppenwallner, G:. Neutral density and crosswind determination from arbitrarily oriented multiaxis accelerometers on satellites. Journal of Spacecraft and Rockets, 47(4): 580–589, 2010. doi:10.2514/1.48114, 2010

Drob, D. P., Emmert, J. T., Meriwether, J. W., Makela, J. J., Doornbos, E, Conde, M., Hernandez, G., Noto, J., Zawdie, K. A., McDonald, S. E., Huba, J. D., and Klenzing, J. H.: An update to the Horizontal Wind Model (HWM): The quiet time thermosphere, Earth and Space Science, 2, 301-319, 10.1002/2014EA000089, https://doi.org/10.1002/2014EA000089, 2015

~~Emmert, J. T., Faivre, M. L., Hernandez, G., Jarvis, M. J., Meriwether, J. W., Niciejewski, R. J., Sipler, D. P., and Tepley, C. A.: Climatologies of nighttime upper thermospheric winds measured by ground-based Fabry-Perot interferometers during geomagnetically quiet conditions: 1. Local time, latitudinal, seasonal, and solar cycle dependence, J. Geophys. Res., 111, A12302, doi:10.1029/2006JA011948, 2006a~~

Emmert, J.T., Hernandez, G., Jarvis, M. J., Niciejewski, R. J., Sipler, D. P., and Vennerstrom, S.: Climatologies of nighttime upper thermospheric winds measured by ground-based Fabry-Perot interferometers during geomagnetically quiet conditions: 2. High-latitude circulation and interplanetary magnetic field dependence, J. Geophys. Res., 111, A12303, doi:10.1029/2006JA011949, 2006b.

Fiori, R. A. D., Koustov, A. V., Boteler, D. H., Knudsen, D. J., & Burchill, J. K.: Calibration and assessment of Swarm ion drift measurements using a comparison with a statistical convection model. Earth, Planets and Space, 68(1), 100. http://doi.org/10.1186/s40623-016-0472-7, 2016.

Forbes, J. M., Roble, R. G., and Marcos, F. A.: Magnetic activity dependence of high–latitude thermospheric winds and densities below 200 km, J. Geophys. Res., 98, 13,693–13,702, 1993.

Ford, E.A.K., Aruliah, A.L., Griffin, E.M., McWhirter, I.: High time resolution measurements of the thermosphere from Fabry-Perot Interferometer measurements of atomic oxygen, Annales Geophys., 25, 1269 – 1278, 2007.

Förster, M., Rentz, S., Köhler, W., Liu, H., and Haaland, S. E.: IMF dependence of high-latitude thermospheric wind pattern derived from CHAMP cross-track measurements, Ann. Geophys., 26, 1581–1595, 2008.

Förster, M., Haaland, S.E., and Doornbos, E., Thermospheric vorticity at high geomagnetic latitudes from CHAMP data and its IMF dependence, Ann. Geophys., 29, 181-186, doi:10.5194/angeo-29-181-2011, 2011.

Förster, M., and Cnossen, I.: Upper atmosphere differences between northern and southern high latitudes: The role of magnetic field asymmetry, J. Geophys. Res. Space Physics, *118*, 5951–5966, doi:10.1002/J.Geophys.Res.a.50554, 2013.

Förster, M., Doornbos, E., and Haaland S.: The role of the upper atmosphere for dawn-dusk differences in the coupled magnetosphere-ionosphere-thermosphere system", in: Dawn-Dusk Asymmetries in Planetary Plasma Environments, eds. Stein Haaland, Andrei Runov and Colin Forsyth, John Wiley Publications, AGU Geophysical Monograph, Vol. 230, 125-142, ISBN: 978-1-119-21632-2, 2017.

Förster, Matthias; Doornbos, Eelco (2019): Upper thermosphere neutral wind cross-track component deduced from CHAMP accelerometer data. GFZ German Research Centre for Geosciences. http://doi.org/10.5880/GFZ.1.1.2019.001

Foster, J. C., Holt, J. M., Musgrove, R. G., and Evans, D. S.: Ionospheric convection associated with discrete levels of particle precipitation, Geophys. Res. Lett., 13, 656, 1986.

Fuller-Rowell, T. J.: Modelling the solar cycle change in nitric oxide in the thermosphere and upper mesosphere, J. Geophys. Res., 98, 1571, 1992.

Fuller-Rowell, T.J., Rees, D.: Interpretation of an Anticipated Long-Lived Vortex in the Lower Thermosphere Following Simulation of an Isolated Substorm, Planet. Space Sci., 32, 69-85, 1984

Fuller-Rowell T.J., Evans, D.S.: Height Integrated Pedersen and Hall Conductivity Patterns Inferred from the TIROS-NOAA Satellite Data, J. GEOPHYS. RES., 92, 7606-7618, 1987

Fuller-Rowell, T. J., Rees, D., Quegan, S., Moffett, R. J., Bailey, G.J.: Simulations of the seasonal and UT variations of the thermosphere and ionosphere using a coupled, three-dimensional, global model, Pur. A. Geoph., 127, 189–217, 1988.

Fuller-Rowell, T. J., Rees, D., Quegan, S., Moffett, R. J., Codrescu, M. V., and Millward, G. H.: A coupled thermosphere ionosphere model, Solar terrestrial energy program (STEP), handbook of ionospheric models, (Ed) Schunk, R. W., 1996.

Gillies, M. D., Knudsen, D., Donovan, E., Jackel, B., Gillies, R., Spanswick, E.: Identifying the 630 nm auroral arc emission height: A comparison of the triangulation, FAC profile, and electron density methods, J. Geophys. Res. Space Physics, 122, doi:10.1002/2016JA023758, 2017.

Griffin, E.M., Aruliah, A. L., Müller-Wodarg, I. C. F., Aylward, A. D.: Comparison of High-Latitude Thermospheric Meridional Winds II: Combined FPI, Radar and Model Climatologies, Ann. Geophys, 22, 863-876, 2004.

Griffin, E. M., Müller-Wodarg, I. C. F., Aruliah, A., and Aylward, A.: Upper thermospheric neutral wind and temperature measurements from an extended spatial field, Ann. Geophys., 26, 2649– 2655, 2008.

Harang, L.: The mean field of disturbance of polar geomagnetic storms, Terr. Mag. Atmos. Elec., 51, 353-380, 1946.

Harris, M.: A New Coupled Middle Atmosphere and Thermosphere General Circulation Model: Studies of Dynamic, Energetic and Photochemical Coupling in the Middle and Upper Atmosphere. PhD Thesis, University of London, 200~~17.~~

Harris, M. J., Arnold, N. F., and Aylward, A. D.: A study into the effect of the diurnal tide on the structure of the background mesosphere and thermosphere using the new coupled middle atmosphere and thermosphere (CMAT) general circulation model, Ann. Geophys., 20, 225–235, doi:10.5194/angeo-20-225-2002, 2002.

Hecht, E., Zajac, A.: Optics, Addison-Wesley Publishing Company, 1980.

Hedin A. E., Salah, J. E., Evans, J. V., Reber, C. A., Newton, G. P., Spencer, N. W., Kayser, D. C., Alcayde, D., Bauer, P., Cogger, L., McClure, J. P.: A Global Thermospheric Model Based on Mass Spectrometer and Incoherent Scatter Data MSIS 1. N_2 Density and Temperature, J.Geophys.Res., 82, 2139-2147, 1977.

Hedin A.E., Biondi, M. A., Burnside, R. G., Hernandez, G., Johnson, R. M., Killeen, T. L., Mazaudier, C., Meriwether, J. W., Salah, J. E., Sica, R. J., Smith, R. W., Spencer, N. W., Wickwar, V. B., Virdi, T. S.:

Formatted: Font: (Default) Times New Roman

Revised Global Model of Thermospheric Winds Using Satellite and Ground-Based Observations, J. Geophys. Res. Space Physics, 96, 7657-7688, 1991.

Hedin, A. E., et al. (1996), Empirical wind model for the upper, middle and lower atmosphere, J. Atmos. Terr. Phys., 58, 1421–1447, doi:10.1016/0021-9169(95)00122-0.

Helleputte, T. V., Doornbos, E., and Visser, P.: CHAMP and GRACE accelerometer calibration by GPS-based orbit determination. Advances in Space Research, 43(12), 1890–1896. http://doi.org/10.1016/j.asr.2009.02.017, 2009.

Hood, R. K. E., Effects of field-aligned currents in the ionosphere-thermosphere system, PhD Thesis, University College London, UK, 2018

Jacchia, L. G., and Slowey, J. W.: A supplemental catalog of atmospheric densities from satellite-drag analysis (No. 348). SAO Special Report, 1972.

Killeen, T. L., Smith, R. W., Hays, P. B., Spencer, N. W., Wharton, L. E., McCormac, F. G.: Neutral winds in the high latitude winter F-region: Coordinated observations from ground and space, Geophys. Res. Lett., 11, 311-314, 1984.

Killeen T.L., Won, Y.-I., Niciejewski, R.J., Burns, A.G.: Upper Thermosphere Winds and Temperatures in the Geomagnetic Polar Cap: Solar Cycle, Geomagnetic Activity and IMF Dependencies, J. Geophys. Res., 100, 21327-21342, 1995.

Koustov, A. V., Lavoie, D. B., Kouznetsov, A. F., Burchill, J. K.,Knudsen, D. J., & Fiori, R. A. D., A comparison of cross-track ion drift measured by the Swarm satellites and plasma convection velocity measured by SuperDARN. Journal of Geophysical Research: Space Physics, 124, 4710-4724. https://doi.org/10.1029/2018JA026245, 2019.

~~Link, R., Cogger, L.L.: A re-examination of the O I 6300A nightglow, J. Geophys. Res., 93, 9883-9892, 1988.~~

Liu, H., Lühr, H., Henize, V., and Köhler, W.: Global distribution of the thermospheric total mass density derived from CHAMP, J. Geophys. Res., 110, A04301, doi:10.1029/2004JA010741, 2005.

Liu, H., Lühr, H.,Watanabe, S., Köhler,W., Henize, V., and Visser, P.: Zonal winds in the equatorial upper thermosphere: Decomposing the solar flux, geomagnetic activity, and seasonal dependencies, J. Geophys. Res., 111, A07307, doi:10.1029/2005JA011415, 2006.

Liu, H., Doornbos, E., & Nakashima, J.: Thermospheric wind observed by GOCE: Wind jets and seasonal variations. Journal of Geophysical Research: Space Physics, 121(7), 6901–6913. http://doi.org/10.1002/2016JA022938, 2016.

Liu, X., Xu, J., Yue, J. & Vadas, S. L., Numerical modeling study of the momentum deposition of small amplitude gravity waves in the thermosphere, Annales Geophysicae, 31(1), 1-14, 2013

Makela, J. J., Meriwether, J. W., Huang, Y., Sherwood, P. J.: Simulation and analysis of a multi-order imaging Fabry-Perot interferometer for the study of thermospheric winds and temperatures, Applied Optics, 50, 4403-4416, 2011.

March, G., Doornbos, E. N. and Visser, P. N. A. M.: High-fidelity geometry models for improving the consistency of CHAMP, GRACE, GOCE and Swarm thermospheric density data sets, Advances in Space Research, 63, 213-238, 10.1016/j.asr.2018.07.009, 2018.

Formatted: Font: Times New Roman, 10 pt

Formatted: Font: Times New Roman, 9 pt

Formatted: No Spacing, Justified, Indent: Left: 0 cm, Hanging: 0.5 cm, Line spacing: 1.5 lines

Formatted: Font: 10 pt

Formatted: Font: 10 pt

Formatted: Font: 10 pt

Formatted: Font: 10 pt

Formatted: Font: 10 pt

Formatted: Font: 10 pt

Formatted: Font: 10 pt

Formatted: Font: 10 pt

Formatted: Font: 10 pt

Formatted: Default Paragraph Font, Font: Calibri, 10 pt

Formatted: Font: 10 pt

Formatted: Font: 8 pt

Formatted: Font: (Default) Times New Roman, 10 pt

Formatted: Font: 9 pt

Formatted: Font: (Default) Times New Roman, 10 pt

Formatted: Font: 9 pt

March, G., E. N. Doornbos, and P. N. A. M. Visser, High-fidelity geometry models for improving the consistency of CHAMP, GRACE, GOCE and Swarm thermospheric density data sets, Advances in Space Research, 63, 213-238, 10.1016/j.asr.2018.07.009, 2019

Marcos, F. A. and Forbes, J. M.: Thermospheric wind from the satellite electrostatic triaxial accelerometer system, J. Geophys. Res., 90, 6543–6552, 1985.

McWhirter I., Rees, D., Greenaway, A. H.: Miniature Imaging Photon Detectors III.~An Assessment of the Performance of the Resistive Anode IPD, J. Phys. E.: Sci. Instrum., 15, 145-150, 1982.

McWhirter, I., Electron Multiplying CCDs - New Technology for Low Light Level Imaging, Proceedings of 33rd Annual European Meeting on Atmospheric Studies by Optical Methods, IRF Sci. Rep., 292, 61-66, 2008.

Mehta, P. M., Walker, A. C., Sutton, E., & Godinez, H. C.: New density estimates derived using accelerometers on-board the CHAMP and GRACE satellites. Space Weather, 15(4), 558–576. http://doi.org/10.1002/2016SW001562, 2017.

Moe, Mildred. M., Wallace, Steven D., Moe, Kenneth : The upper mesosphere and lower thermosphere, A review of experiment and theory, Geophysical Monograph 87, 1995

Quegan, S., Bailey, G. J., Moffett, R. J., Heelis, R. A., Fuller-Rowell, T. J., Rees, D., and Spiro, A. W.: A theoretical study of the distribution of ionisation in the high-latitude ionosphere and the plasmasphere: First results of the mid-latitude trough and the light ion trough, J. Atm. Terr. Phys., 44, 619, 1982.

Rees, D., Fuller-Rowell, T. J., Gordon, R., Smith, M. F., Maynard, N. C., Heppner, J. P., Spencer, N. W., Wharton, L., Hays, P. B., and Killeen, T. L.: A theoretical and empirical study of the response of the high latitude thermosphere to the sense of the “Y” component of the interplanetary magnetic field, Planet. Space Sci., 34, 1–40, 1986.

Reigber, C., Lühr, H., and Schwintzer, P.: CHAMP mission status, Adv. Space Res., 30, 129–134, 2002.

Roble, R. G., Ridley E. C., and Dickenson, R. E.: On the global mean structure of the thermosphere, J. Geophys. Res., 92, A8, 8745–8758, 1987.

Ronksley, Amy, Optical remote sensing of mesoscale thermospheric dynamics above Svalbard and Kiruna, PhD thesis, UCL, London, UK., 2016.

Salah, J. E. and Holt, J. M.: Midlatitude thermospheric winds from incoherent scatter radar and theory, Radio Sci., 9, 301–313, 1974.

Schlegel, K., Lühr, H., St.-Maurice, J.-P., Crowley, G., and Hackert, C.: Thermospheric density structures over the polar regions observed with CHAMP, Annales Geophysicae, 23, 1659–1672, 2005.

Shepherd, S. G.: Altitude-adjusted corrected geomagnetic coordinates: Definition and functional approximations, J. Geophys. Res. Space Physics, 119, doi:10.1002/2014JA020264, 2014.

Sica R. J., Rees, M. H., Roble, R. G., Hernandez, G., Romick, G. J.: The Altitude Region Sampled by Ground-Based Doppler Temperature Measurements of the OI 15867K Emission Line in Aurorae, Planet. Space Sci., 34, 483-488, 1986.

~~Smith, R. W., Sweeney, P. J.: Winds in the thermosphere of the northern polar cap, Nature **284**, 437 – 438, doi:10.1038/284437a0, 1980.~~

Formatted: Font: Times New Roman, 10 pt

Song, P., Vasyliūnas, V. M., and Zhou, X.-Z.: Magnetosphere-ionosphere/thermosphere coupling: Self-consistent solutions for a one-dimensional stratified ionosphere in three-fluid theory, J. Geophys. Res., 114, A08213, doi:10.1029/2008JA013629, 2009.

Song, P., and Vasyliūnas, V. M.: "Inductive-dynamic coupling of the ionosphere with the thermosphere and the magnetosphere", in: 'Modeling the Ionosphere-Thermosphere System', edited by J. Huba, R. Schunk, and G. Khazanov, American Geophysical Union, Washington DC,10.1029/2012GM001308, Geophysical Monograph Series 201, 201-215, 2013.

Sutton, E. K., Nerem, R. S., & Forbes, J. M.: Density and Winds in the Thermosphere Deduced from Accelerometer Data. Journal of Spacecraft and Rockets, 44(6), 1210–1219. http://doi.org/10.2514/1.28641, 2007.

Tapley, B.D., Bettadpur, S., Watkins, M., and Reigber, C.: The gravity recovery and climate experiment: Mission overview and early results, Geophys. Res. Lett., 31, L09607, DOI: 10.1029/2004GL019920, 2004.

Torr, M. R., Richards, P. G., and Torr, D. G.: A new determination of ultraviolet heating efficiency in the thermosphere, J. Geophys.Res., 85, 6819, 1980a.

Torr, M. R., Richards, P. G., and Torr, D. G.: The solar ultraviolet heating efficiency in the mid-latitude thermosphere, Geophys.Res. Lett., 6, 673, 1980b.

Vadas, S. L. and Crowley, G.: Neutral wind and density perturbations in the thermosphere created by gravity waves observed by the TIDDBIT sounder, J. Geophys. Res. Space Physics, *122*, 6652–6678, doi:10.1002/2016JA023828, 2017.

Visser, T., March, G., Doornbos, E., de Visser, C., & Visser, P.: Horizontal and vertical thermospheric cross-wind from GOCE linear and angular accelerations. Advances in Space Research. http://doi.org/10.1016/j.asr.2019.01.030, 2019.

Vlasov, M. N., Nicolls, M. J., Kelley, M. C., Smith, S. M., Aponte, N., and Gonzalez, S. A: Modeling of airglow and ionospheric parameters at Arecibo during quiet and disturbed periods in October 2002, J. Geophys. Res., 110, A07303, doi:10.1029/2005JA011074, 2005.

Yiu, H.C.I: High latitude thermosphere meso-scale studies and long-term database investigations with the new Scanning Doppler Imager and Fabry-Perot Interferometers, Ph.D. Thesis, Univ. of London, London, UK, 2014.

21st August 2019

We would like to thank the reviewers for their time taken to read and feedback very helpful advice and comments on our paper. Our responses are below.

We have added an extra figure (Figure 3) to illustrate the geometry of the CHAMP ascending and descending orbits, and the projection of the FPI wind vectors onto the CHAMP cross-track direction.

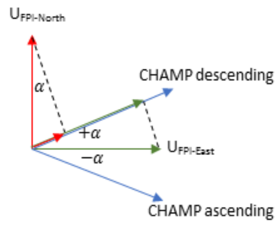

Figure 3: Geometry illustrating the projection of FPI look direction wind components onto the CHAMP cross-track direction for the ascending and descending tracks.

This is in response to both referees requesting that we do this projection for a fairer comparison with the CHAMP cross-track winds. This has required a renumbering of the figures as shown in the table below:

Original Figure Number	**New Figure Number**
1 CHAMP solar max 2001-2003 Longyearbyen	1 CHAMP solar max 2001-2003 Longyearbyen
2 CHAMP solar max 2001-2003 Kiruna	2 CHAMP solar max 2001-2003 Kiruna
3 CHAMP solar max 2005-2007 Longyearbyen	3 geometry for projecting FPI winds onto CHAMP cross-track direction
4 CHAMP solar max 2005-2007 Kiruna	4 CHAMP solar max 2005-2007 Longyearbyen
5 FPI solar max and min 2001-2003 Longyearbyen	5 CHAMP solar max 2005-2007 Kiruna
6 FPI solar max and min 2001-2003 Kiruna	6 FPI solar max and min 2001-2003 Longyearbyen
7 CHAMP vs HWM87 and HWM90 and FPIs	7 FPI solar max and min 2001-2003 Kiruna

measurements made by UCL + Alaska (1980)	
8 CHAMP vs FPI for 2- <= Kp < 4+ for Longyearbyen and Kiruna	8 CHAMP vs HWM93 and FPIs measurements made by UCL + Alaska (1980)
9 frequency distribution of CHAMP/FPI for solar max and both Longyearbyen and Kiruna	9 CHAMP vs FPI for 2- <= Kp < 4+ for Longyearbyen and Kiruna
10 CMAT2 model demonstration of effects of changing viscosity	10 frequency distribution of CHAMP/FPI for solar max and both Longyearbyen and Kiruna
11 height profiles of CMAT2 model zonal winds and comparison with the red line emission intensity profile.	11 CMAT2 model demonstration of effects of changing viscosity
12 frequency distribution of Kp	12 height profiles of CMAT2 model zonal winds and comparison with the red line emission intensity profile.
13 CMAT2 zonally averaged winds at Longyearbyen and Kiruna	13 frequency distribution of Kp
14 global maps of CMAT2 zonal winds comparing winds at 240 km with height integrated winds	14 CMAT2 zonally averaged winds at Longyearbyen and Kiruna
15	15 global maps of CMAT2 zonal winds comparing winds at 240 km with height integrated winds

Responding to Ref 1 comment 2 has also meant a re-numbering of the remaining equations:

Original Equation Number	**New Equation Number**
1	deleted
2	deleted
3	deleted
4	**1**
5	**2**
6	**5** (corrected original number which was out of order)
7	**3**

8	**4**

Some additional points we noted:

We noted that Figure 12 required some more explanation of the simulations of the height profile of the zonal winds (lines 633-645):

"Figure 12 illustrates how ground-based FPIs make measurements of the neutral winds at 240 km altitude. The left plot shows a height profile of the CMAT2 zonal mean zonal winds at the latitude of Longyearbyen. There are 6 simulations to demonstrate the effect on the height profile of the zonal mean zonal winds when changing the viscosity. CMAT2 uses a viscosity term that is the weighted mean divided by the scale height of two coefficients of viscosity: the molecular viscosity μ_m; and the turbulent viscosity μ_t. The simulations represent a comparison with the original molecular viscosity (dark blue). The other lines are for low (yellow - divided by 100) and high molecular viscosities (pink - doubled). The low and high turbulent viscosities are represented by the Prandtl numbers 0.7 (red) and 100 (green), where 2 is the default value used in CMAT2; which is relevant for the height at which gravity waves deposit momentum (Liu et al., 2013). The light blue line labelled "Mata" is an intermediate profile. As can be seen, the molecular viscosity dominates in the thermosphere above 100 km and at the altitudes where the FPI is measuring. The dark blue and yellow lines are representative of a vertical slice of Figure 11 left and right, respectively, for the latitude of Longyearbyen."

Replaced Nov-Jan with DOY 300-65 in abstract and line 424. This is the correct range of DOY used in the FPI selection criteria, as well as the CHAMP data.

Added the following:

i) an extra affiliation for MF
ii) data availability
iii) Co-author Rosie Hood's recently awarded PhD thesis as a reference

Moved and consolidated description of red line emission profile and winds with respect to height to follow Figure 12.

Anonymous Referee #1: Interactive comment on Ann. Geophys. Discuss., https://doi.org/10.5194/angeo-2019-57, 2019. (Received and published: 31 May 2019)

Dear Editor, I have reviewed the paper by Aruliah et al. titled "Comparing high-latitude thermospheric winds from FPI and CHAMP accelerometer measurements." The paper describes polar observations from FPIs and the CHAMP satellite. Observations from different instruments are compared and discrepancies discussed. It is important to the community to understand the differences between the FPI and CHAMP observed thermospheric winds. CHAMP winds are known to be larger than the FPI measurements.
While the cause for such discrepancy may be unknown at the moment, at least, we should know how the two sets data are different. Hence, the paper is very important and should be considered for publication. It can be a good reference for future users of the two data sets. The paper in the current form, however, has some significant issues need to be addressed.

1. The paper somehow lost focus. It got into too many sub-topics: FPI (old) -FPI (new) differences, HWM87-HWM90 differences. I think for the purpose of understanding the CHAMP and FPI difference, we should avoid using very old data. If the topic were the long-term trend, then we should examine long data string. The value of this paper is on the CHAMP and FPI comparison.

We beg to differ on this comment. It is important to provide a context and full argument for this important finding, i.e. that there is a serious discrepancy between the two methods of measuring thermospheric winds; but that the UCL FPI results are consistent with the U.Alaska FPI. Then the FPI procedure is discussed in section 6.2. However, we have added a sentence (lines 480-481): "These are interannual and inter-solar cycle discussions for a later paper."

The HWM87 and HWM90 plots have been replaced with a single plot using the later version HWM93.

The calibration of FPIs is an important section attempting to understand the discrepancy in the CHAMP-FPI winds. The University of Alaska FPI measurements at Longyearbyen, made in the early 1980s, are used to show that their FPI measurements are consistent in phase with the UCL FPI measurements 20 years later. They are also of a magnitude closer to the UCL FPI than the CHAMP winds. Even then Hedin et al. (1991) noted that the U.Alaska ground-based FPI zonal wind magnitudes in 1980 showed smaller magnitudes than satellites.

2. The section L67-89 has some major issues. The thermospheric dynamics is governed by the momentum, energy, and continuity equations. It cannot be expressed in the formulas listed in the section. CHAMP's larger winds do not necessarily lead to larger temperatures. Smaller FPI winds are not always connected to the lower temperatures. We cannot use temperature to verify wind values.

Agreed that this is a very simplified argument, but the purpose is to highlight the repercussions of overestimating the neutral wind when dividing energy between heating and acceleration of the neutral gas. But considering the referee's concerns, we have decided to remove lines 67-92 and replace with a general comment on the partitioning of energy (lines 65-71):

"With incorrect scaling, there arises a problem of distortion of energy budget calculations of the upper atmosphere. A precise estimation of energy supply to the system is hindered essentially, because the partitioning of kinetic and thermal energy channels becomes obscured. The acceleration of the neutral air in 3-D space with respect to the active driver of the plasma motion is important to estimate, for instance, the Joule heating rate as one of the most important thermal energy inputs. This has a knock-on effect on the calculation of the absolute density of the gas, which is an important parameter used in, for example, satellite orbit calculations."

Removal of these paragraphs and 3 equations has required re-numbering of the remaining equations as outlined in the table above.

3. I am lost in the section L279 – L316. I understand that the CHAMP cross-track winds are not aligned with the eastward direction on the ground. The angle is different for the ascending and descending nodes. The angles are +/- 7.2 deg and +/-13.3 deg for KEOPS and Longyearbyen (ascending and descending). So the obvious thing to do is to compare separately the ascending and descending nodes. Use the ground based meridional and zonal components to compute the wind value along the direction of CHAMP cross-track measurement (mostly to add the contribution from the meridional winds). I don't understand why that was not done. I do not see an argument to let me believe that I can ignore the viewing angle difference between the ground based zonal wind and CHAMP cross track winds. So I suggest the authors use the ground based FPI data to form the wind values along the CHAMP cross-track direction to do a direct comparison. Or alternatively, using the CHAMP ascending and descending node measurements to remove the contribution from the meridional wind and compute the zonal wind. Hopefully, that would give you better comparison between the FPI and CHAMP observations.

The FPI vector winds have been projected on the cross-track direction for the ascending (East - alpha) and descending (East + alpha) as suggested. The discrepancy in magnitude is still large. An extra Figure (new Fig 3) has been added to illustrate the geometry.

4. Figure 7 should be the focus of the paper. I really don't see much value having two HWM model runs results shown here. You only need one. The FPI (Alaska) probably does not add much and more likes a distraction. The old and new FPI comparison should be discussed in a different paper, you can have inter-annual variations here.

The two HWM models have been replaced with the later HWM93 model. The FPI (Alaska) data remains because it shows that the UCL FPI data are consistent with the Alaska FPI under fairly similar f10.7 and mean Kp. Indeed Hedin et al (1991) had noticed a systematic discrepancy between satellite and ground-based FPI winds even then.

5. The solar minimum data are not very useful since there are no CHAMP observations.

The original Figs 3 and 4 (now called Figs 4 and 5) show CHAMP data from solar minimum.

6. I think the conclusion should be clearer that the CHAMP winds are overestimated. As the paper points out that the CHAMP winds are almost the same magnitude as ion drift at Kiruna, which is incorrect.

Agreed. This point is discussed in Section 6 for various aspects such as the role of viscous action in the upper thermosphere (Sect. 6.1) or the ion-neutral comparisons (Sect. 6.4). To accentuate this set of problems, we emphasized this with a expanded paragraph referring to the Fiori et al (2016) Swarm measurements of ion velocities (lines 767-774), and two additional sentences at the end of the Conclusions (lines 834-837). This is a key point for further discussions and also for more modelling/simulation studies (lines 837-839).

"Fiori et al (2016) compared ion velocities measured by the Electric Field Instrument on Swarm with the CS10 statistical ionospheric convection model by Cousins and Shepherd (2010) which is based on 8 years of data

(1998-2005) collected by 16 SuperDARN coherent scatter radars. The climatology represented by the CS10 model in Fiori et al's Figure 3a indicates speeds in the few hundreds of ms^{-1}, while the instantaneous values along the Swarm satellite pass (their Figure 3d) show much stronger drift peak values on the resolution level of seconds or shorter. Even after allowing for offsets, their 1-sec resolution corrected cross-track ion drifts achieve horizontal velocities well over 1,000 ms^{-1}, which probably indicates the highly dynamic behaviour in the auroral regions compared with quasi-stable conditions used for empirical models. However, recently Koustov et al. (2019) compared the Swarm cross-track ion drifts with the SuperDARN radar network and found that the Swarm ion velocities are a factor of 1.5 larger. They suggest reasons for the disparity, including refining the calibration of Swarm and the differences in spatial/temporal resolution."

"We may also need to rethink the procedure of comparing different spatial and temporal resolutions of in-situ satellite versus remote ground-based FPI measurements in terms of the geometry of cross-track winds at high latitudes."

7. While Aruhiah et al. 2005 reference is listed for the instrument information. It will be a great help to give a short paragraph on the two FPIs (gaps, aperture size, detector, from which year to which years) given that instrument upgraded over the years.

Added to section 5.2.

Minor

1. In the comparison section, the FPI (Alaska) was used, but there is no mention of it in the abstract and earlier instrument description. It should be added to the abstract, if it is to be used. Personally, I think the data should be dropped.

The U.Alaska FPI measurements at Longyearbyen illustrate that the UCL FPI measurements 20 years later are consistent. They are a reference measurement, so do not need to appear in the abstract.

2. Many the figures have very low resolution and are difficult to read.

Figures 5-8 have been increased in size on the page. In particular, Figs 5 and 6 have been split so that a,b and c,d are on 2 separate pages. (These are now re-labelled Figs 6-9)

3. Figure 5, the FPI from one direction has error bars and the other does not. Why?

Only one set of error bars were included for the sake of clarity of the plots. However, we have now included the error bars for all the FPI look directions.

4. L 444 to LL448. 'During the 1980s and 1990s we used state-of-the-art UCL designed and built Imaging Photon Detectors (McWhirter et al., 1981) and then EMCCDs (Andor iXon 887/885) were installed around 2005 (McWhirter, 2008). The revolution over the last 30 years in : : :' Was the UCL FPI running with the imaging photon detector from 2001 to 2003, it is not clear in the paper. That is why I ask for a more detailed instrument description to be added.

We have added some more explanation in section 5.2, in particular the dates of changes of etalon. The etalon gap is important in the calibration of the measured Doppler shift to wind calculation, which is described in section 6.2. The effect of the detector is to improve the sensitivity to the photon counting by electon multiplying. This reduces the error of measurement. It does not change the calibration of the wind speeds (lines 445-459).

"During the 1980s and 1990s we used state-of-the-art UCL designed and built Imaging Photon Detectors (McWhirter et al., 1982). Astrocam Antares cameras replaced the IPD in the Svalbard FPI from 1998, and in the KEOPS 630 nm FPI in 2002. However, these cameras had the disadvantage of slow readout times which were essential for the best noise performance and so time resolution was compromised. In 2003 the first Electron Multiplying CCDs revolutionised low light level imaging. These cameras combined superior signal to noise ratio with very fast readout times. The first one was put into service at KEOPS in 2003, followed by Svalbard in 2005 (McWhirter, 2008). The huge advancement over the last 30 years in low light detectors has allowed atmospheric gravity wave observations using exposure times as little as 10 seconds at auroral latitudes (Ford et al., 2007). Note that the upgrade of the detector is to improve the photon sensitivity which reduces the error of measurement. It does not change the calibration of the wind speeds.

Any changes of etalon required re-calibration of the measured Doppler shift to calculate winds, as discussed in section 6.2. The KEOPS FPI used a 10 mm etalon gap up to January 2002, when it was replaced with an 18.5 mm gap etalon. Then in January 2003 a 14 mm etalon was put in, which has been there until the present time. For the Longyearbyen FPI there was a 14 mm etalon until April 2005, which was replaced with an 18.5 mm etalon from September 2005 until the present time."

5. I do not see Harris 2001 paper (L554) in the reference. Or the reference date is wrong? It is not 2017, should it be 2001?

Yes, my typo mistake. The reference is to the Harris PhD thesis in 2001.

6. Equ. 5 is wrong. It does not match the two references.

The coefficient of viscosity is based on Dalgarno and Smith (1962), where it is given as

viscosity = $3.34 \text{x} T^{0.71}$ micropoise

Equation 5 is the conversion to SI units. The Banks and Kockarts reference is removed.

7. There should be some discussion on hypothesis C (L520).

Hypothesis C – the assumptions of the FPI and CHAMP measurement techniques are discussed in sections 6.1-6.3. A sentence has been added to make this explicit.

8. Why is the HWM model run not included in Figure 8 comparison for Kiruna?

The HWM93 model has been run for both Longyearbyen and Kiruna and appears in the renumbered Figs 8 and 9.

We have removed old Fig 8a (Longyearbyen 15 min averages) and instead the renumbered Fig 9 shows only the Kiruna zonal winds as 1 hour averages, to match the Longyearbyen 1 hour averages shown in the renumbered Fig 8.

Anonymous Referee #2 Interactive comment on Ann. Geophys. Discuss., https://doi.org/10.5194/angeo-2019-57, 2019. (Received and published: 31 May 2019)

This paper statistically compares upper thermospheric F-region winds measured by two high-latitude ground-based Fabry-Perot Interferometers (one located near Kiruna and other at Longyearbyen) and derived from in-situ accelerometer measurements onboard the CHAMP satellite. One of the ground-based stations is located in the auroral zone whereas the other one is in the polar cap. Results show that CHAMP winds are systematically 1.5-2 times larger than FPI winds. Further, the authors utilize the existing modeling tools for exploring the various possible reasons responsible for these systematic discrepancies in winds obtained from in-situ and optical techniques. Overall, this study can serve as an important reference for data users of these instruments.

In my view, the manuscript is loosely written. There is some repetitiveness of some of the text and the manuscript could be streamlined quite a bit. I would strongly recommend the authors to make clear, elaborate, and explain the following parts:

1. Please explain the purpose of having fist four figures (Figures 1-4). I think they are irrelevant and can be dropped without impacting the focus of the paper. Instead, it would help focusing this study on the core topic - FPI and CHAMP wind comparison.

The CHAMP figures 1-4 and FPI Figs 5-6 will be valuable to modellers to show phase and amplitude of the seasonal variation of thermospheric winds in the polar cap and auroral region for the European sector. Note these have been renumbered as in the table at the top. The FPI can only measure night-time winter winds. This is the reason why satellite measurements are so important.

2. Line 17: should be kinematic viscosity instead of viscosity?

Molecular viscosity dominates in the thermosphere, so this has been made explicit throughout.

3. Line 25: +-2 degrees in latitude, longitude, or both? Please explain.

The radial distance is the horizontal equivalent of +/- 2 deg in latitude (i.e. ~220km horizontal radius) at 240 km altitude.

4. Line 148: In Table 1 (column 4 and row 2), you mean 1.860 UT?

Yes, thank you. Corrected

5. Line 172: Emmert 2006a reference is not valid here because it is a climatological study.

Ok, thanks, point taken. Emmert ref removed

6. Lines 299-317: The simplest and most direct way to compare CHAMP and ground station winds would be to project ground station winds along the CHAMP cross track winds; it is doable because both the zonal and meridional winds exist for ground station FPIs.

This has been done for Figures 7 and 8 (renumbered 8 and 9) and to determine the ratios of CHAMP/FPI along the cross-track direction shown in the histogram in Fig 9 (renumbered 10).

7. Figure 5 and 6: Please keep the figure titles consistent. Subfigures a/b titles are not consistent with c/d titles: one shows Kp index in title and others not. In addition,

please keep consistency when using plus or minus symbols in Kp values. For example, sometimes the manuscript uses Kp<2 and the other times Kp<2- [[or Kp<2o (line 367, 413, etc.) which may be a typo]]. Kp<2o is also present in Figures 6a and b. Moreover, I would suggest using an actual math symbol (ï˝C ˇc) instead of <=.

The <= has been replaced and the titles made consistent.

8. Lines 424-426 are referred to which figure/figures?

This is clarified in the text: ("The general trends seen in the northern winter CHAMP zonal winds (Figures 1-4, renumbered 1,2,4,5) are also seen in the FPI winds (Figures 5-6, renumbered 6-7). The phases match extremely well for both sites, however, there is a considerable difference in magnitude. The next 2 figures 7-8 (renumbered 8-9) show direct comparisons of CHAMP and FPI winds along the cross-track direction.")

9. Figure 7:
- This comparison is done for Kp 2-4, whereas earlier figures and discussion was focused on Kp 0-2. Same is true for Figure 8. Please explain the reason for this gear shift.

There is a lot of modelling effort into studying the active ionosphere-thermosphere, so we wanted to show this too. In particular it is relevant to the comparison with high latitude ion velocities discussed in section 6.4.

- Please explain why HWM87 and HWM90 were used instead of HWM14? HWM14 is the latest version of this empirical wind model.

HWM93 is used to replace HWM87 and HWM90

10. Figure 9: In addition to this figure, a plot showing CHAMP/FPI ratio as a function of UT or LT would be really helpful.

This is a very good idea, and has been added to Fig 9 (renumbered 10)

11. Lines 518-522: The major source of discrepancies could be the assumptions used when applying different wind extraction schemes as they can fail under different conditions.

Indeed, this is the point of sections 6.1-6.3. Sentence added to make this explicit just before section 6.1 (lines 554-555):
"With respect to hypothesis C – the assumptions of the FPI and CHAMP measurement techniques are discussed in the following sections 6.1-6.3."

12. Line 556: Please verify the viscosity expression.

The coefficient of viscosity is taken from Dalgarno and Smith (1962). Here it is given as

viscosity = 3.34x$T^{0.71}$ micropoise

Equation 5 is the conversion to SI units. The Banks and Kockarts reference is removed.

13. Lines 715-722: Project FPI wind vector along the CHAMP cross track wind component.

Done, including an additional illustration of the geometry (figure 3). Words added, including (lines 752-754): ". To deal with this the UCL FPI zonal winds observed to the East and West are projected onto the CHAMP ascending and descending cross-track directions, and then averaged into 1-hour bins, thus replicating the CHAMP zonal wind averages (see Figures 7 and 8)."

14. Section 6.4: I did not get the motive of adding this section. So, please state explicitly the contribution of this section in this investigation.

This is a very important argument. At high latitudes the average neutral wind at high latitudes is expected to be smaller than the ion velocities, since the latter are driven by the magnetospheric dynamo. This is stated in the 2nd sentence of this section.